Journal of Sedimentary Research

LARGE-SCALE BLEACHING OF RED BEDS RELATED TO UPWARD MIGRATION OF HYDROCARBONS: LOS CHIHUIDOS HIGH, NEUQUÉN BASIN, ARGENTINA

ANA L. RAINOLDI,[1,2,3] MARTA FRANCHINI,[1,2] DANIEL BEAUFORT,[4] PATRICIA PATRIER,[4] ADOLFO GIUSIANO,[5] AGNES IMPICCINI,[1,2] AND JOSEFINA PONS[1,2]

[1]Consejo Nacional de Investigaciones Científicas y Técnicas, Centro Patagónico de Estudios Metalogenéticos, Argentina
[2]Departamento de Geología y Petróleo, Facultad de Ingeniería, Universidad Nacional del Comahue, Buenos Aires 1400, (8300) Neuquén, Argentina
[3]Departamento de Geología, Universidad Nacional del Sur, San Juan 670, (8000) Bahía Blanca, Argentina
[4]Université de Poitiers, IC2MP, CNRS-UMR 7285, Hydrasa, Bâtiment B08, Rue Albert Turpin, F-86022 Poitiers Cedex, France
[5]Subsecretaría de Minería e Hidrocarburos, Irigoyen 436, Piso 4, (8300) Neuquén, Argentina
e-mail: analaurarl@hotmail.com

ABSTRACT: The striking arrangement of colorful facies in the sandstones outcrops of the Los Chihuidos high, Argentina, has been attributed to the surface expression of hydrocarbon-induced alteration. The Huincul Formation (late Cenomanian–early Turonian) is part of the thick continental red-bed-dominated Neuquén Group, which consists of meandering fluvial deposits developed in a foreland basin. Visual distinctions reveal four diagenetic facies: red, white, gray, and minor brown sandstones. Differences in the diagenetic mineralogy among sandstones facies are interpreted to depend on the degree of interaction with hydrocarbon-bearing solutions and the relative position of the redox roll front developed during this process. The red facies represents the original oxidized sandstone, with hematite, kaolinite, quartz and albite overgrowths, and calcite cement precipitated under oxidizing conditions during the regional burial diagenesis. The white facies formed during the interaction of red beds with reduced fluids (in presence of hydrocarbons or organic acids), where clasts and cement were partially dissolved, and iron was reduced to Fe^{2+} due to redox reactions and removed, resulting in the sandstone decoloration and in a marked development of the secondary porosity. Minor montmorillonite replaced kaolinite and detrital feldspars, and a poikilotopic calcite precipitated, filling the pores. The gray and the brown sandstone bound the redox front, which is characterized by the presence of abundant clay minerals and oxide minerals enriched in vanadium and copper. Montmorillonite and secondary hematite are dominant in the more oxidized gray sandstones whereas interstratified chlorite–montmorillonite is more abundant in the more reduced brown sandstones. The coexistence of these minerals indicates metastable reducing–oxidizing conditions at the redox front. Based on diagenetic characteristics, tectonic framework, maturation timing of source rocks, and petroleum-emplacement history, hydrocarbons could have migrated into the Huincul Formation during the Tertiary uplift, but later erosion could have released the hydrocarbons and exhumed the reservoir.

This multi-scale investigation of diagenetic features related to burial history and to structure-controlled upflow of hydrocarbons in a succession of siliciclastic rocks enhances modeling of a regional-scale redox system worldwide. Our study offers new insight into the application of authigenic minerals to trace hydrocarbon pathways along red beds and to evaluate the reservoir quality, in the understanding the importance of fluid compositions, mixing, and fluid–rock interaction along a major redox system.

INTRODUCTION

The Neuquén Basin (124.000 km^2; Fig. 1) is the largest gas producer and the second largest oil producer in Argentina with 2075.5 million barrels of oil and 17 tcf (trillion of cubic feet) of gas of discovered resources (Giusiano et al. 2011 and references therein). The Los Chihuidos high (LCh; Fig. 1) is one of the most prominent structures in the Neuquén Basin, and has a complex geological and tectonic history. Late Cretaceous (Cenomanian–Campanian) red beds of the Neuquén Group (Cazau and Uliana 1973) are widely exposed along the flanks of LCh (Fig. 2A, B). Striking color variations linked to red-bed decoloration are obvious in sandstones outcrops of the Huincul Formation (late Cenomanian–early Turonian, Legarreta and Gulisano 1989) in LCh

(Giusiano and Bouhier 2009; Rainoldi et al. 2012a). Bleaching of red beds has been described in other sectors of the Neuquén Basin (Giusiano et al. 2006, 2008; Pons et al. 2009, 2012), and in hydrocarbon reservoirs worldwide (Levandowski et al. 1973; Surdam et al. 1993; Schumacher 1996; Chan et al. 2000; Garden et al. 2001; Beitler et al. 2003, 2005; Parry et al. 2009). This phenomenon has been attributed to redox reactions between hematite from the red beds and hydrocarbon-bearing solutions (Surdam et al. 1993; Beitler et al. 2005; Schöner and Gaupp 2005). Experimental demonstration of this process has also been reported in the laboratory (Shebl and Surdam 1996). One interpretation of the widespread bleached outcrops of the Huincul Formation in LCh suggests that hydrocarbon-bearing fluids migrated through these Cretaceous sandstones. Subsequent uplift and erosion of the Chihuidos structure
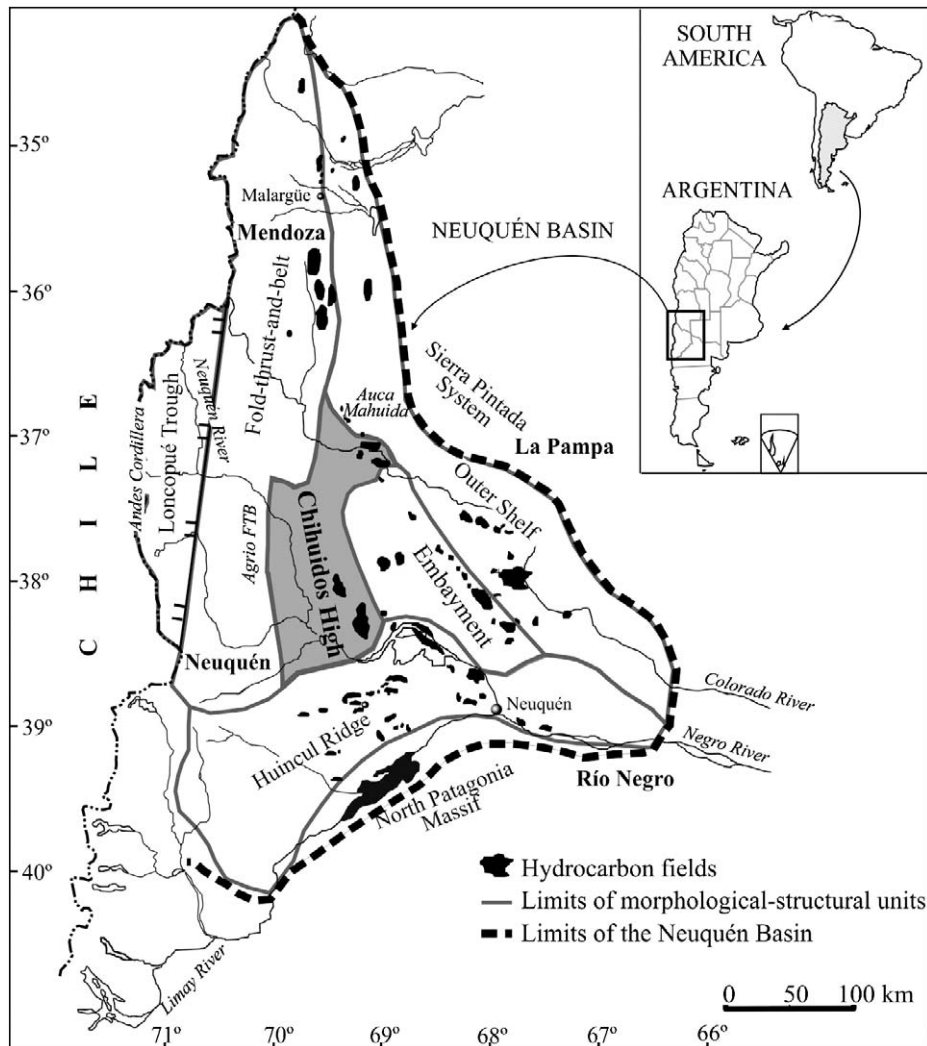
Fɪɢ. 1.—Map of the Neuquén Basin of Argentina, showing the main structural units and the location of hydrocarbons fields (modified from Giusiano and Bouhier 2009).

destroyed the traps, liberated the hydrocarbons, and exhumed the reservoir.

A succession of parallel canyons that cut across the main axis of the structure shows outcrops of the Huincul Formation with uninterrupted exposures for more than 10 km long and 80 m thick. An area of 4.5 km long × 9 km wide (Fig. 2C, D, E) was selected for this study to determine the geochemical and physical processes responsible for the decoloration of the red-bed outcrops in LCh. For this purpose, the study integrates observations of: (1) broad-scale patterns of alteration evident in satellite images, (2) mineralogical and textural changes between the red beds and the bleached facies, (3) chemical composition of the red bed, bleached facies, and their main minerals (seven stratigraphic profiles have been measured), and (4) element mobility during the decoloration event. This multi-scale study of patterns of bleaching in a succession of siliciclastic rocks reveals a regional-scale redox system linked to structure-controlled upflow of hydrocarbons and associated fluids, and the chemical reactions between reducing fluids and diagenetic minerals.

Regional Geology

The Neuquén Basin is a retroarc foreland basin located in west-central Argentina, surrounded by the North Patagonian massif, the Sierra Pintada, and the Andes Cordillera (Fig. 1). The tectonic evolution of this basin began in the Late Triassic and Early Jurassic driven by extensional collapse of the Permian–Triassic orogenic belt, accommodated by a southwest-oriented extensional stress field (Vergani et al. 1995). Several episodes of structural inversion occurred, but the most significant of them (and with a northwest orientation) was in the late Oxfordian–earliest Kimmeridgian, which marked the reorganization of extensional stress fields related to the fragmentation of southwestern Gondwana and the Atlantic opening (Vergani et al. 1995). This tectonic evolution is reflected in the stratigraphic record of the basin with the development of source and reservoir hydrocarbon zones. The Neuquén basin records at least 220 My of basin subsidence with 7,000 m of Upper Triassic–Cenozoic basin infill. The principal morphological–structural units of the Neuquén basin are the following: 1) External fold-and-thrust belt, 2) Outer Shelf, 3) Huincul Ridge, 4) Los Chihuidos high, and 5) Embayment (Fig. 1).

The Los Chihuidos high represents a 70-km-long, basement-cored asymmetric anticline characterized by a sharp western forelimb and a gently extended eastern back limb, overlain by a series of secondary folds developed along its axis (Mosquera and Ramos 2006). It is flanked to the northeast by the Auca Mahuida volcano, to the southeast by the Añelo trough, to the south by the Huincul Ridge, and to the west by the Agrio fold-and-thrust belt (Fig. 1).

The Los Chihuidos high uplift has been explained as tectonic inversion of Triassic half grabens (Precuyan) in a foreland basin (Cristallini et al.
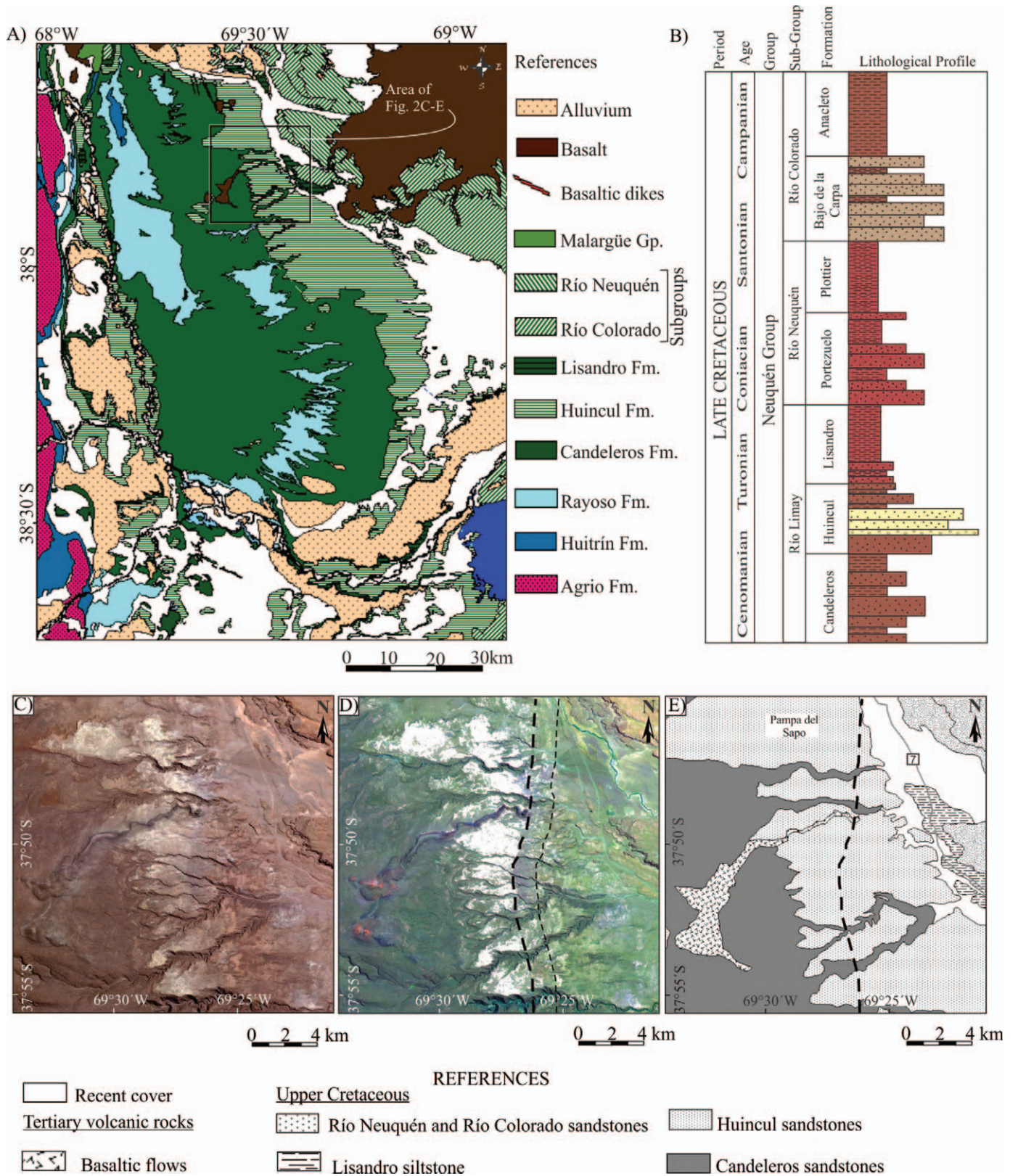
FIG. 2.—**A)** Geological map of Los Chihuidos high in the central Neuquén Basin. **B)** Stratigraphic column of the Neuquén Group (after Sánchez et al. 2008). **C)** True color composition Landsat ETM-RGB 321 of Pampa del Sapo zone. **D)** Landsat ETM-RGB 741 illustrates changes in the distribution of iron, enhancing the presence of the migrating front. Superimposed is the Supervised Classification limiting the bleached outcrops. Dotted line indicates the migration front, which moves towards the east and separates bleached from red sandstones. An intermediate hue between both (see second thinner dotted line), indicates a transitional passage from altered to unaltered outcrops. **E)** Lithological map of the study area located in Pampa del Sapo, in the west flank of Los Chihuidos high.
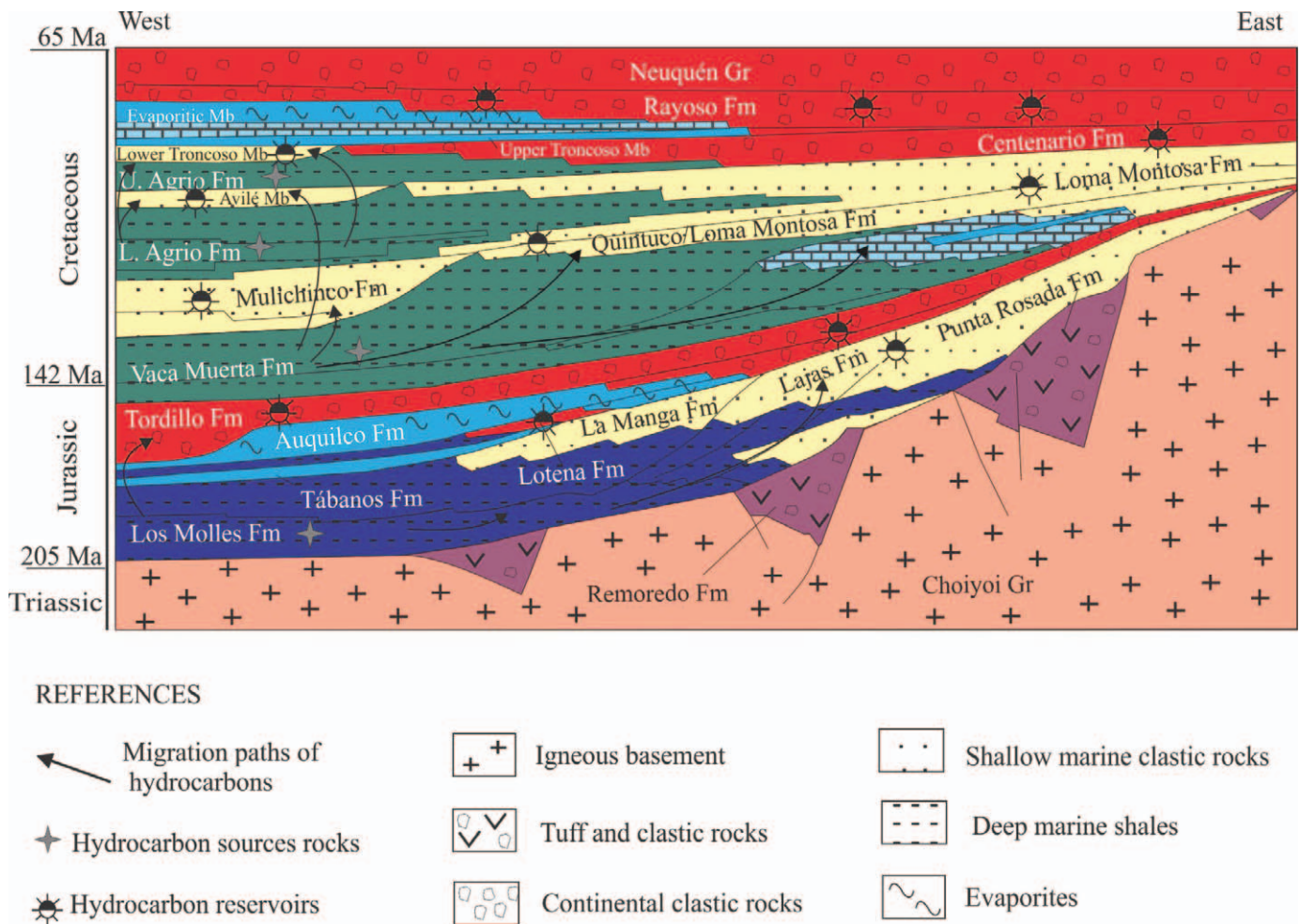
FIG. 3.—Cross section showing main source rocks and hydrocarbon reservoirs in the Neuquén Basin (after Legarreta et al. 1999).

2005; Maretto and Pángaro 2005). Maretto and Pángaro (2005) suggested the occurrence of a Berriasian–Valanginian compressive tectonic event that was associated with the deformation of the Huincul high, represented in LCh by marked bed thinning of the Quintuco and Vaca Muerta formations. Mosquera and Ramos (2006) interpreted a transpressive inversion linked to oblique subduction during the Jurassic to Early Cretaceous (Sinemurian–Valangian), associated with a change in the convergence vectors in the subduction zone between oceanic and continental plates.

The Late Cretaceous stage was characterized by a reactivation pulse with westward contraction in the Agrio fold-and-thrust belt, which caused a low-angle intra-Cenomanian unconformity at the top of the the Rayoso Formation and the deposition of 1,300 m of synorogenic red beds of the Neuquén Group (Cazau and Uliana 1973) (Fig. 2B). The age of the lower part of the synorogenic sequence was estimated by zircon fission-track dating in the Huincul Formation to be 88 ± 3.9 Ma (Corbella et al. 2004) and ~ 90 Ma by fission-track dating on apatites (Zamora Valcarce et al. 2009). The U/Pb age of detrital zircons of the Candeleros Formation (98 Ma; Tunik et al. 2008) suggests that the deformation of the Agrio fold-and-thrust belt began after 98 Ma. This event has been explained by the eastward migration of the magmatic arc toward the foreland, and its reestablishment in the western part of the Agrio fold-and-thrust belt linked to a relative shallowing of the Nazca plate (Ramos and Folguera 2005; Ramos and Kay 2006). Deformation may have started in the inner

part of the Agrio fold-and-thrust belt during Late Cretaceous, but it has migrated towards the foreland to affect the current Los Chihuidos high in the Late Cretaceous–early Paleocene (Zamora Valcarce et al. 2009).

During the Maastrichtian–Eocene (70–50 Ma), uplift eroded 1,000 m of sedimentary deposits (Zamora Valcarce et al. 2009). The presence of deformed middle Miocene synorogenic deposits in LCh suggests that the block again was uplifted by tectonic inversion of normal faults during the late Miocene (Mosquera and Ramos 2006). Apatite fission-track dating identified two Miocene cooling and uplift events: the first at 20–25 Ma, and the second at 14 Ma, with the erosion of 700 and 750 m of sediments, respectively (Zamora Valcarce et al. 2009). These data coincide with the second tectonic event of Neogene age proposed by Maretto and Pángaro (2005), which has been responsible for the present-day configuration of LCh.

Post-tectonic volcanism is represented by radial subvolcanic dikes of the Desfiladero Formation (Ramos and Barbieri 1989), emplaced in extensional zones transverse to the main axis folds (Ardolino and Franchi 1996). Ramos (1981) inferred an age of 9 Ma for the dikes forming the Desfiladero Formation based on the ages of similar dikes in Aguada San Roque (Ugarte 1976), considerably younger than the new ^{40}Ar/^{39}Ar age of 25 ± 4 Ma for the dike forming the Desfiladero Negro ridge (Kay and Copeland 2006).

During the Pliocene, extensional reactivation of faults inverted during the Miocene coincided with the eruption of the small, intraplate, alkali-
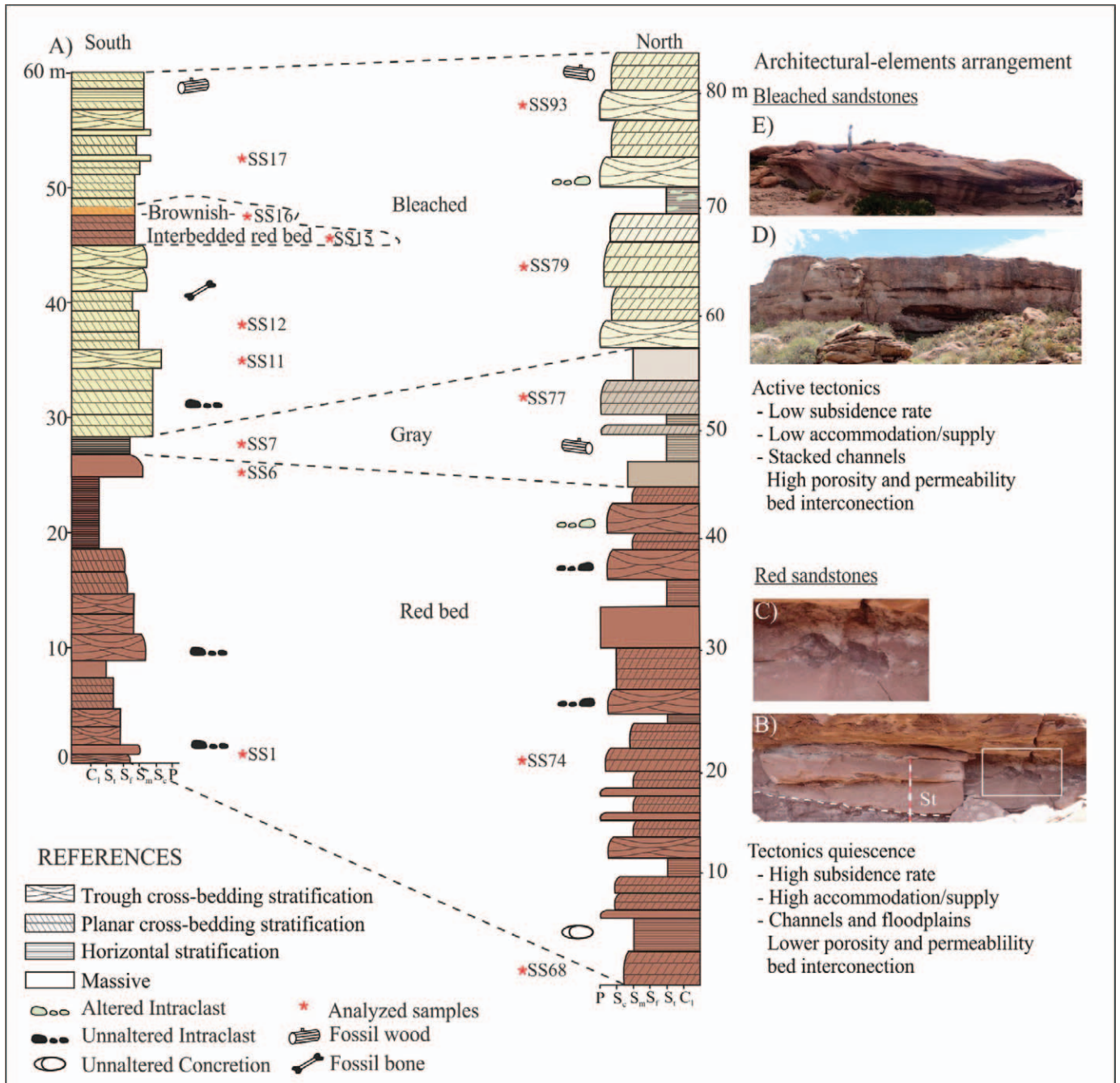
FIG. 4.—**A)** Stratigraphic profiles I (right) and II (left) of the Huincul Formation, showing the distribution and transitions of the diagenetic facies. C_l, clay; S_t, silt; S_f, fine-grained sand; S_m, medium-grained sand; S_c, coarse-grained sand; P, pebble. Connection of stratigraphy with tectonics is shown: **B, C)** red sandstones are preserved in a sequence with low sediment supply and high accommodation rates, developed during tectonic quiescence characterized by channel and floodplain deposits. **D, E)** Bleached sandstones correspond to high-energy system related to active tectonics with high sediment supply and low accommodation rate, resulting in high-permeable stacked channels.

basalt cones of Parva Negra (K/Ar of 4.5 Ma ± 0.5 Ma; Ramos and Barbieri 1989) and Cerro La Horqueta. Finally, Pleistocene–Holocene normal faulting and basic alkaline, intraplate volcanism (Kay et al. 2004) formed the Auca Mahuida monogenic volcano to the east (1.38/1.78 Ma ± 0.07/0.14 Ma; Kay et al. 2004). Quaternary movements were recognized by Cristallini et al. (2005) and Messager et al. (2010), in the last case supported by geomorphologic studies of terraces from the Neuquén River.

The Hydrocarbon System

The Neuquén basin contains five petroleum systems of different importance through Mesozoic strata that include transgressive and regressive cycles responsible for the distribution of source rocks, reservoirs, and seals (Vergani et al. 2011) (Fig. 3). The Neuquén Embayment (Fig. 1) hosts the main hydrocarbon kitchen of the basin, from which oil and particularly gas migrated (Legarreta et al. 1999). The

TABLE 1.—*Whole-rock chemical composition of representative samples from the red, white, gray, and brown facies of the Huincul Formation.*

Facies	Red	Red	Red	Red†	Red†	Gray	Gray	Brown	White	White	White	White	White
Sample	240410-SS1	240410-SS6	010411-SS68	240410-SS15	010411-SS74	240410-SS7	010411-SS77	240410-SS16	240410-SS11	240410-SS12a	240410-SS17	010411-SS79	020411-SS93
SiO_2	66.96	78.24	74.64	85.53	78.18	76.43	75.59	82.25	84.33	66.46	72.18	82.24	77.75
Al_2O_3	11.83	10.88	12.09	8.07	9.89	11.13	12.41	8.65	8.55	6.25	6.54	8.68	10.43
TiO_2	0.49	0.28	0.39	0.10	0.20	0.39	0.26	0.15	0.13	0.09	0.09	0.20	0.30
FeO	0.22	0.47	0.89	0.76	0.54	0.74	0.79	1.13	0.14	0.22	0.10	0.76	0.33
Fe_2O_3	3.36	1.76	1.19	0.41	0.85	1.68	1.52	0.91	0.53	0.25	0.59	0.33	0.36
MnO	0.12	0.02	0.04	0.01	0.02	0.02	0.02	0.03	0.13	0.10	0.15	0.01	0.09
CaO	5.68	0.78	1.77	0.61	1.55	0.90	1.14	0.71	0.61	12.90	9.50	1.46	0.91
MgO	0.30	0.36	0.46	0.20	0.23	0.52	0.71	0.99	0.16	0.11	0.25	0.52	0.44
Na_2O	4.50	3.79	4.73	2.61	3.78	3.57	3.95	2.35	2.68	2.14	2.01	2.69	3.13
K_2O	0.93	1.05	1.19	1.35	1.21	1.12	1.28	1.39	1.25	0.99	1.23	1.38	1.05
P_2O_5	0.11	0.03	0.07	0.03	0.05	0.06	0.04	0.05	0.03	0.03	0.04	0.04	0.07
LOI	4.96	1.22	1.72	1.07	1.46	2.13	3.04	2.20	1.27	10.44	8.18	2.27	3.86
Total	99.49	98.93	99.27	100.80	98.02	98.78	100.80	100.90	99.83	100.00	100.90	100.70	98.76
V	89.00	84.00	45.00	32.00	53.00	639.00	817.00	61.00	30.00	17.00	25.00	29.00	65.00
Cu	20.00	100.00	40.00	<20	20.00	<20	30.00	100.00	<20	90.00	<20	60.00	>10000
U	1.55	2.17	1.95	1.35	1.33	3.50	5.02	4.55	4.75	3.31	2.11	1.82	27.80

† Red bed partially altered.

TABLE 2.—*REE of representative samples from the red, white, gray, and brown facies of the Huincul Formation.*

| Facies	Red	Red	Red	Red†	Red†	Gray	Gray	Brown	White	White	White	White	White
Sample	240410-SS1	240410-SS6	010411-SS68	240410-SS15	010411-SS74	240410-SS7	010411-SS77	240410-SS16	240410-SS11	240410-SS12a	240410-SS17	010411-SS79	020411-SS93
La	15.40	17.20	27.00	16.80	20.00	18.50	19.20	19.40	19.20	14.30	18.70	21.00	14.90
Ce	32.20	32.20	50.50	32.80	38.80	34.80	35.90	37.40	40.50	29.70	36.00	41.60	28.40
Pr	3.69	3.58	6.56	3.51	4.84	3.79	4.41	4.06	4.40	3.20	3.97	4.92	3.44
Nd	14.30	13.30	24.40	13.00	18.20	14.30	16.20	14.60	16.90	12.00	14.60	18.40	12.70
Sm	2.84	2.38	4.37	2.30	3.31	2.57	3.02	2.78	3.15	2.25	2.76	3.46	2.45
Eu	0.80	0.62	0.94	0.55	0.78	0.69	0.77	0.63	0.79	0.58	0.63	0.77	0.60
Gd	2.24	1.79	3.03	1.71	2.47	1.89	2.36	1.86	2.37	1.79	2.17	2.42	1.88
Tb	0.33	0.26	0.46	0.24	0.37	0.28	0.39	0.27	0.35	0.26	0.34	0.37	0.35
Dy	1.93	1.56	2.39	1.36	1.86	1.67	2.18	1.58	2.01	1.48	2.01	1.94	1.94
Ho	0.38	0.32	0.48	0.26	0.38	0.34	0.47	0.30	0.37	0.27	0.39	0.38	0.41
Er	1.11	1.01	1.40	0.81	1.14	1.11	1.45	0.92	1.09	0.78	1.08	1.13	1.16
Tm	0.17	0.16	0.23	0.12	0.17	0.18	0.23	0.15	0.16	0.12	0.16	0.18	0.19
Yb	1.21	1.11	1.52	0.83	1.10	1.21	1.54	0.99	1.14	0.83	1.03	1.20	1.20
Lu	0.20	0.19	0.23	0.14	0.16	0.21	0.23	0.17	0.19	0.14	0.17	0.18	0.18

† Red bed partially altered.
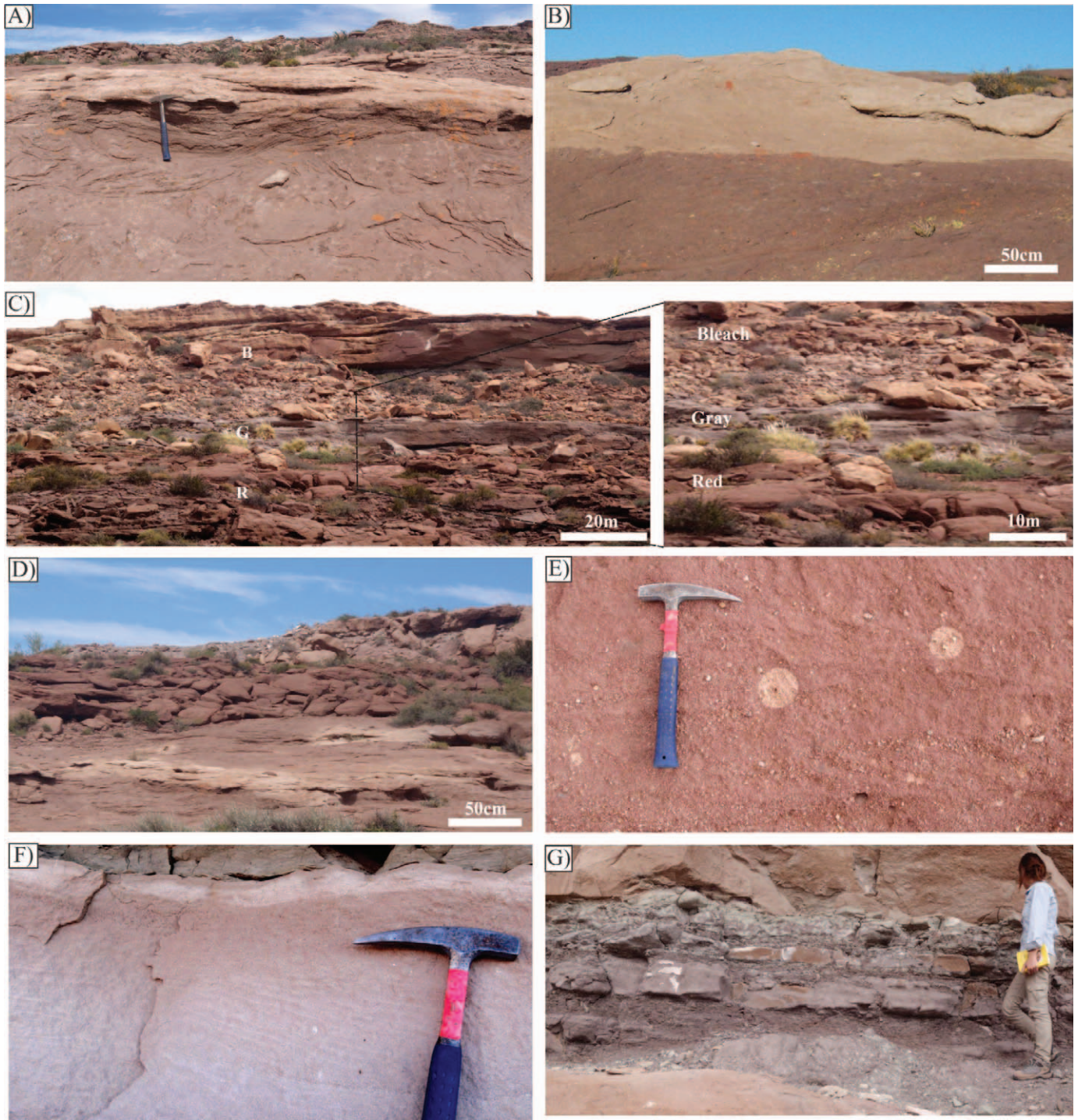
FIG. 5.—**A, B)** Transition from red to bleached within strata parallel to bedding. **C)** Vertical transition with red beds at the base (R), gray in the middle (G), and bleached at the top (B). **D)** Reduction spots as evidence of localized reduction during pervasive reddening (Bensing et al. 2005). **E)** Stratigraphic anisotropies like bounding and lamination surfaces. **F)** Impermeable fine-grained red beds within coarse-grained bleached sandstone.

petroleum system encompasses a pod of active source rock and all genetically related oil and gas accumulations, which includes the geologic elements and processes that are essential for oil and gas accumulation (Magoon and Beaumont 1999). The petroleum systems in the embayment are Los Molles (Toarcian)–Lotena (Bajocian) and Vaca Muerta (Tithonian)–Sierras Blancas/Tordillo (Kimmeridgian), both of which source very light oil and gas. Hydrocarbons generated in Los Molles are mainly methane and are hosted in the Lajas and Lotena formations (Legarreta et al. 1999). In the second system, gas and condensate have been produced from the Vaca Muerta Formation and accumulated in the Sierras Blancas Formation, whereas very light oils were hosted in the Quintuco and Mulichinco formations (Legarreta et al. 1999). Since the late Albian, Vaca Muerta source rocks have been in the oil generation window, but recently have evolved into the gas window (Legarreta et al.

TABLE 3.—*Average for detrital grains and maximum and minimun diagenetic minerals and porosity in all diagenetic sandstones of the Huincul Formation.*

Detrital grains	Red		White		Gray		Brown	
Monocrystalline quartz	24.98		25.00		23.99		23.02	
Polycrystalline quartz	4.76		4.65		4.07		4.51	
Plagioclase	26.98		25.86		26.34		25.15	
K-Feldspar	2.10		2.93		3.60		3.57	
Igneous rock fragments	36.92		35.15		39.57		43.74	
Metamorphic rock fragments	4.25		4.15		2.44		0.00	
Sedimentary rock fragments	0.00		2.32		0.00		0.00	
	Red		White		Gray		Brown	
Diagenetic minerals (vol. %)	Max.	Min.	Max.	Min.	Max.	Min.	Max.	Min.
Hematite	3.30	0.40	0.59	0.25	1.50	0.50	traces	0.00
Kaolinite	7.00	traces	9.00	traces	6.00	traces	7.00	traces
Quartz overgrowths	2.00	0.59	1.50	0.40	1.00	traces	0.40	traces
Albite overgrowths	0.50	0.27	0.41	0.10	0.42	0.16	0.35	0.05
Calcite	8.15	0.00	21.84	0.00	0.50	0.00	traces	0.00
	Red		White		Gray		Brown	
Porosity	Max.	Min.	Max.	Min.	Max.	Min.	Max.	Min.
Intergranular porosity	11.80	7.43	23.27	0.00	17.20	####	17.00	13.79
Intragranular porosity	0.72	0.00	0.66	0.00	2.04	1.44	0.52	0.13

1999; Chebli et al. 2011). In LCh, the evaporites from the Auquilco Formation (thickness up to 300 m) behave as a barrier for hydrocarbon migration from Los Molles source (Legarreta et al. 2008). Thus, most of the hydrocarbon accumulations from the Vaca Muerta–Mulichinco system are gas, including Aguada Pichana, Sierra Chata, and Parva Negra fields (Anechine et al. 2002; Bringworth et al. 2011). Mulichinco accumulations were fed from the Vaca Muerta Formation source by vertical migration (Rooney et al. 1999).

Stratigraphy

Late Cretaceous continental sedimentary rocks (Rayoso Formation and Neuquén Group) and subordinate Tertiary volcanic units (Parva Negra, La Horqueta, and Desfiladero formations) crop out in LCh (Fig. 2A). The Neuquén Group was deposited in the Late Cretaceous foreland basin during the uplift of the Agrio fold-and-thrust belt. The Group constitutes a sedimentary succession 1,300 m thick, divisible into three subgroups and seven formations, from bottom to top: Candeleros, Huincul, and Lisandro formations of the Río Limay Subgroup, Portezuelo and Plottier formations of the Río Neuquén Subgroup, and Bajo de la Carpa and Anacleto formations of the Río Colorado Subgroup (Fig. 2B) (Ramos 1981). The following paragraphs summarize the main characteristics of the sedimentary succession that crops out in the study area (Candeleros, Huincul, and Lisandro formations of the Río Limay Subgroup; Fig. 2A–E).

The Río Limay Subgroup (De Ferrariis 1968) comprises 350 m of Cenomanian to middle Turonian fluvial deposits. The Candeleros Formation (Keidel in Herrero Ducloux 1946) is composed mainly of fine-grained red sandstones interlayered with red mudstones. These strata include a markedly coarse-grained succession of conglomeratic beds deposited in meandering and braided fluvial systems with the development of paleosols and swamp environments (Leanza and Hugo 2001; Sánchez and Cardozo 2002).

The Huincul Formation (Keidel in Herrero Ducloux 1946) (late Cenomanian–early Turonian, Legarreta and Gulisano 1989) (Fig. 4A) is made up of medium to coarse-grained sandstones with sparse intraformational conglomerate beds with locally abundant fossil wood, deposited in a fluvial environment of higher energy than that of the overlying Candeleros Formation. The stratigraphy of the Huincul Formation in the study area records underfill and overfill stages exhibited in two depositional arrangements: a) the lower section, characterized by lateral migration of channel in a well-developed floodplain, and b) the upper section, made up of vertically stacked bodies, with muddy clasts at the base of the stratas and without floodplain deposits (Fig. 4B–E) (Rainoldi et al. 2012b).

The Lisandro Formation (Herrero Ducloux 1939) is a thick succession of red pelitic packages with intercalations of fine-grained sandstones and red and green siltstones. A marked decrease in the energy of deposition may have occurred during the deposition of the Lisandro Formation, suggested by the development of wide alluvial plains (Leanza and Hugo 2001). Variations in sediment supply and accommodation space linked to changes in the subsidence rate are the main control of the Río Limay Subgroup accumulation (see also Garrido 2010; Rainoldi et al. 2012b).

METHODS

Bleached sandstone outcrops were analyzed with Landsat 7 ETM+ scene. From different band combinations, it was empirically determined that color composition RGB 741 enhances the delimitation of the alteration front associated with the red-bed and bleached rocks, obtaining the most useful mapping for this study. The lithofacies characterization and the architectural elements were based mainly on Miall's (1996) code with minor modifications. Color variations were catalogued using the Munsell rock color chart. Representative samples of diagenetic facies from two selected profiles (Fig. 4A) were collected for laboratory analysis.

Samples (n = 40) were analyzed first with a binocular polarizing microscope under transmitted and reflected light. Thin sections with carbonate cement were stained for identification of carbonates. Percent mineralogy was determined by point counting (300 points) on each representative sample of the diagenetic facies. Image analysis quantified modal composition, porosity, and overgrowth cements, using the software JMicroVision V.1.2.7 (Roduit 2008). The data represent an
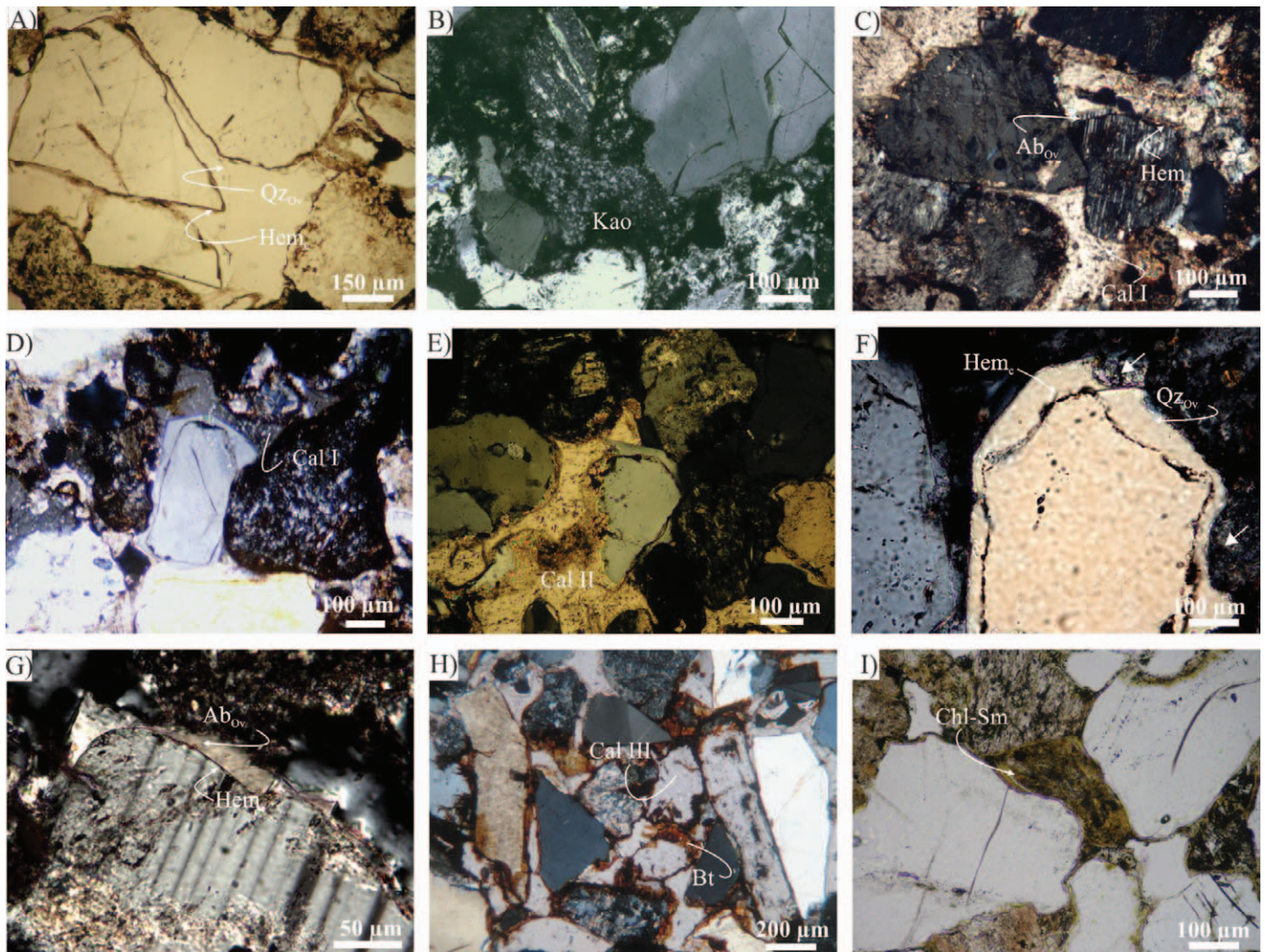
FIG. 6.—Microphotographs of sandstone facies developed during deposition, diagenesis, and alteration. Red facies: **A)** early hematite (Hem) coatings cover all the detrital grains. The presence of quartz overgrowths (Qz_{Ov}) suggests that they were deposited after the formation of hematite coatings but prior to compaction. **B)** Pore-filling kaolinite (Kao). **C)** Albite overgrowths (Ab_{Ov}) on detrital feldspars surfaces above hematite coatings. **D, E)** Calcite I (Cal I) cement in net contact with clasts and previous cements, and calcite II (Cal II) replaces clasts and previous cements. Bleached facies: **F, G)** hematite coatings are preserved beneath quartz and albite overgrowths. Quartz overgrowths are corroded, evidencing partial dissolution (see arrow). **H)** Poikilotopic calcite III (Cal III) is typically impregnated by bitumen. Brown facies: **I)** Yellowish-orange coatings of mixed-layer chlorite–smectite (Chl-Sm).

estimation of the components on 2D images. Samples of the sandstones (n = 13) were analyzed for major, trace, and rare earth elements by inductively coupled plasma emission spectrometry (ICP-ES) and ICP mass spectrometry (ICP-MS), titration for FeO and coulometry for CO_2, at Actlabs Laboratory (Activation Laboratories LTD), in Ontario, Canada (Tables 1, 2).

The minerals were first identified using a Rigaku DMAX-2D diffractometer at the Centro de Investigaciones de Minerales Arcillosos de la Universidad Nacional del Comahue, Neuquén. Bulk samples and the clay fraction (< 2 µm) were analyzed from 2° to 40° 2θ, at 2° 2 /min, with CuKα radiation, run at 40 kV and 20 mA. The XRD reflections were evaluated with Rigaku software. For all samples, clay minerals were identified by XRD of the 2 µm fraction. Whole-rock samples were crushed and ground with a mortar and pestle, and then 30 g of each powdered whole rock were added to one liter of distilled water and as oriented aggregates dispersed by ultrasonic probe. The < 2 µm fraction was separated by timed centrifugation. Oriented preparations of Sr-saturated < 2 µm fraction were analyzed by means of XRD in air-dried

(AD) state (drying at room condition), ethylene glycol (EG) solvation, and heating to 375°C and 550°C for one hour. A second group of samples was analyzed at the Université de Poitiers. Clay size fractions < 4 µm were extracted by sedimentation for oriented and randomly oriented powder mounts. No cation exchange was performed. All clay preparations were analyzed on a Bruker D8 Advance diffractometer. Diffracted beam $CuK\alpha_{1+2}$ radiation was used (40 kV, 40 mA) and collected by a linxeye detector. Relative humidity was not controlled during data acquisition.

Representative samples of each facies were selected for SEM observations which were made on small, freshly fractured bulk rock samples that were coated with carbon. Chemical composition, morphology, and texture of clay-mineral assemblage were studied using a JEOL® 5600 electron microscope equipped with a Bruker energy-dispersive X-ray spectroscopy detector (EDS). Analytical conditions were as follows: accelerating voltage 15 kV, probe current 1 nA, working distance 17 mm, counting time of 100 s. The analyzed elements were Na, Mg, Al, Si, Mn, Fe, Ti, K, and Ca. The microanalysis system was calibrated using
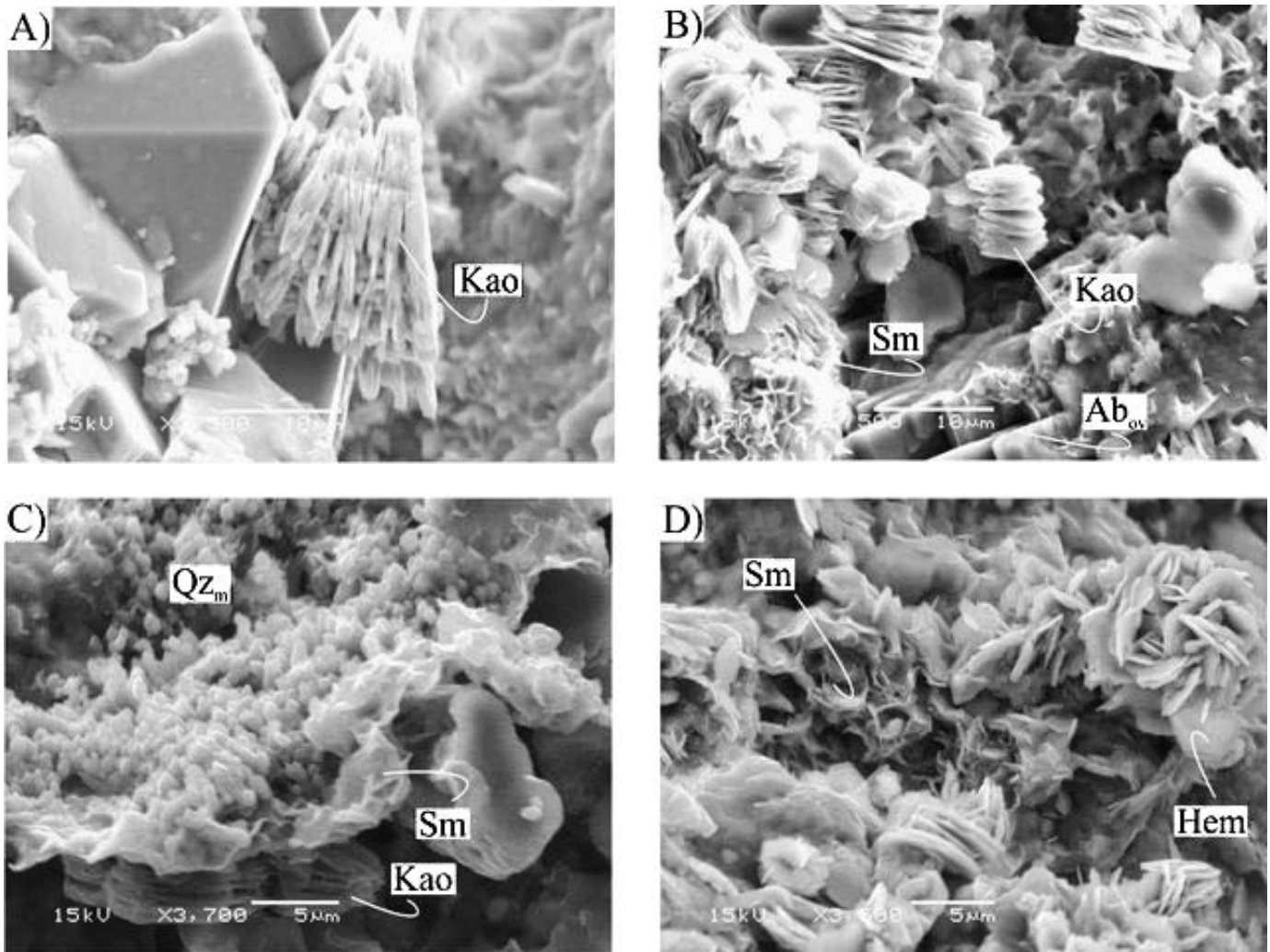
F<small>IG</small>. 7.—Scanning electron microscope images showing clay minerals in the Huincul sandstones. **A)** Books of stacked flakes of kaolinite (red sandstone) without dissolution features. **B)** Ragged edges of kaolinite flakes with partial growing of smectite after kaolinite (bleached sandstone). **C)** Smectite after kaolinite with aggregates of microquartz (gray sandstone). **D)** Secondary V-bearing hematite crystallized in a rosette arrangement (gray sandstone).

synthetic and natural oxides and silicates ($MnTiO_3$, hematite, albite, orthoclase, and diopside), and corrections were made using a ZAF program. The relative errors on the analyzed values are $< 1.5\%$ (except Na which is $> 3\%$). Total Fe was arbitrarily considered as FeO or Fe_2O_3 according to the nature of the analyzed mineral. The chemical compositions of the albite overgrowths (five analyses) were determined at the Electron Microprobe Laboratory, College of Earth, Ocean and Atmospheric Sciences, Oregon State University, USA. These analyses were performed with a Cameca SX-100 electron microprobe equipped with five wavelength-dispersive spectrometers (WDS) and one energy-dispersive spectrometer (EDS) with a thin window for detection of light elements. Operating conditions were 15 kV and 30 nA with a beam diameter of 5 µm.

Mid-infrared (MIR) spectra (400 to 4000 cm^{-1}) of clay material were acquired on KBr pellets using a Nicolet 760 FT-IR spectrometer equipped with a potassium bromide (KBr) beam splitter and DTGS-KBr detector. The resolution was set at 4 cm^{-1} with co-addition of 100 scans. KBr pellets contained 1mg of sample for 150 mg of KBr powder, crushed into a mortar and pressed under 8 tons for 5 minutes in a hydraulic press before drying at 120°C.

RESULTS

Distribution of the Bleached Sandstones in the Huincul Formation

The Landsat satellite image with a RGB 741 combination discriminates bleached strata (Fig. 2C, D). The image reveals a north–south front 20 km long $\times$ 12 km wide with white hues in contact with the original red bed to the west. This front disappears eastward until it reaches another N–S front (Fig. 2D; second thinner dotted line) and grades into the unaltered red bed. In the field, bleached beds alternate with red beds and are commonly placed at the top of them. These observations provided the basis for a supervised classification, in which bleached zones were mapped easily. The effectiveness of the method was corroborated with field observations.

Transitions from red to bleached zones can crosscut stratigraphic boundaries. Color transition can be parallel to bedding, either inside strata units or independent of bedding (Fig. 5A, B); a gray or brown intermediate color of sandstones is present at some contacts at the interface of the red and white sandstones (Fig. 5C). Other types of alteration are typically irregular with dead-ends and re-entrants (Fig. 5D). Spherical reduction spots are evident as well (Fig. 5E); these features could be indicative of
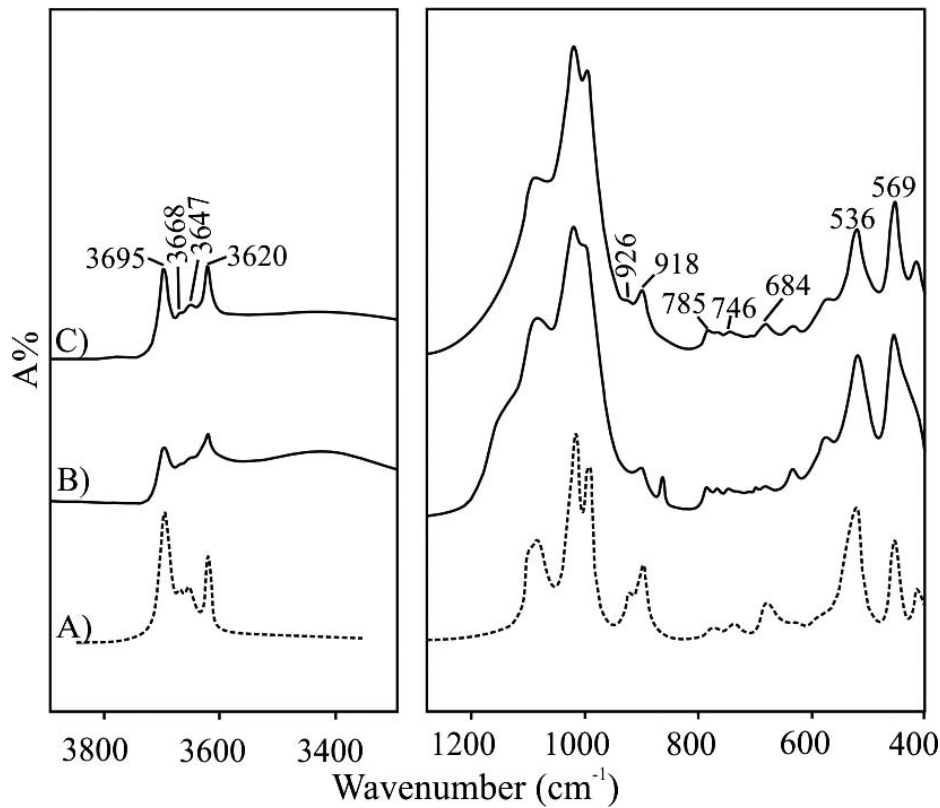
Fig. 8.—The infrared spectra of kaolinite in the red (B) and white (C) sandstones. Absorption peaks of kaolinite in both spectras match perfectly, indicating a unique stage of kaolinite precipitation. In comparison with literature, corresponds to well-ordered kaolinite (A; Madejová et al. 2011).

localized reduction features during early diagenesis (Bensing et al. 2005). A stratigraphic control on bleaching is suggested by decoloration of a) more permeable beds, b) bounding surfaces (Fig. 5F), and c) interconnected beds, not confined by impermeable strata that could have acted as barriers for fluid migration (i.e., beds that are not overlain and underlain by impermeable beds) (Fig. 5G). Interconnected high-energy depositional facies such as amalgamated channels seem to have been preferentially altered (Fig. 4A, B).

Petrography and Modal Mineralogy of the Huincul Formation

The Huincul Formation consists of a very coarse-grained to medium-grained, medium- to well-sorted and texturally immature feldspathic litharenites (Folk et al. 1970) with subordinate fine-grained conglomerates. In both types, the amount of cement varies considerably and includes quartz, feldspar, hematite, calcite, kaolinite, barite, and gypsum and anhydrite. Its porosity depends mainly on the sorting and the presence and

TABLE 4.— *Chemical composition of albite overgrowths.*

Wt percent	1	1	1	1	1	2
SiO_2	70.52	70.35	70.54	68.68	68.80	65.17
TiO_2	0.01	0.00	0.00	-	0.00	0.03
Al_2O_3	21.94	21.79	22.16	21.64	21.41	19.52
Fe_2O_3*	0.03	0.04	0.08	0.02	0.03	0.40
MgO	0.00	0.01	0.00	-	-	0.36
CaO	0.02	0.04	0.03	0.04	0.02	0.15
Na_2O	11.76	11.65	12.11	10.95	11.22	14.28
K_2O	0.02	0.05	0.02	0.04	0.04	0.09
Total	104.30	103.93	104.93	101.38	101.53	100.00
Cations based on 32 oxygens						
Si	11.79	11.81	11.75	11.79	11.81	11.59
Al	4.33	4.31	4.35	4.38	4.33	4.09
Ti	0.00	0.00	0.00	0.00	0.00	0.00
Fe	0.00	0.01	0.01	0.00	0.00	0.05
Mg	0.00	0.00	0.00	0.00	0.00	0.09
Na	1.91	1.90	1.95	1.82	1.87	2.46
Ca	0.00	0.01	0.00	0.01	0.00	0.03
K	0.00	0.01	0.00	0.01	0.01	0.02
Or	0.17	0.55	0.23	0.50	0.47	0.83
Ab	99.67	99.03	99.53	99.08	99.29	97.99
An	0.15	0.42	0.24	0.42	0.24	1.17

[1] Microprobe analysis; [2]SEM-EDS analysis.
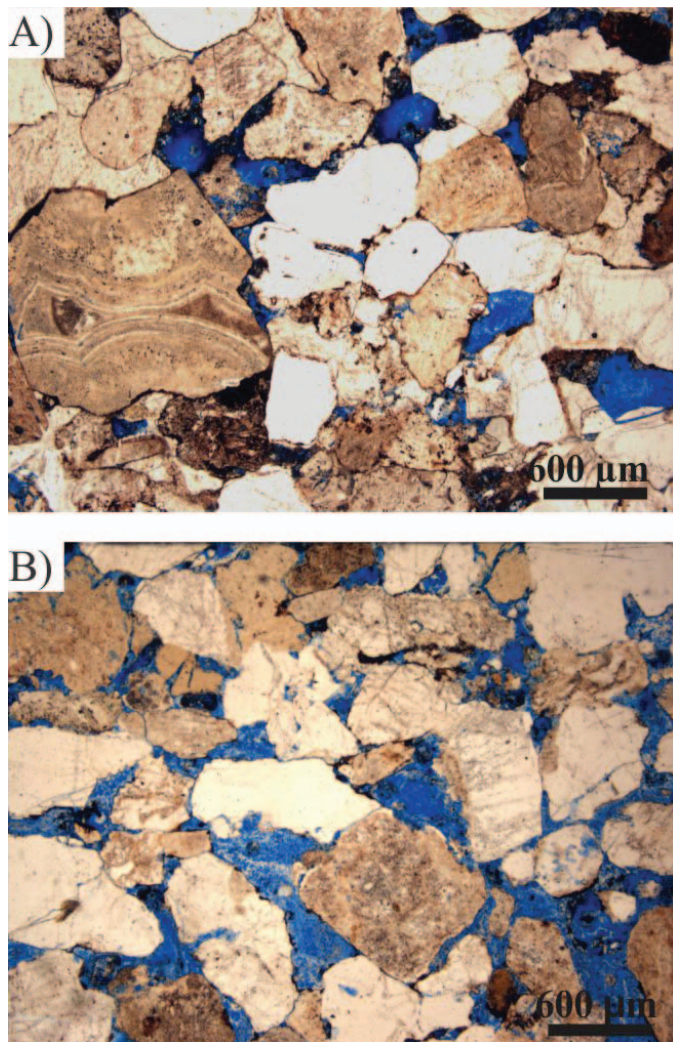* All Fe as Fe^{+3}.

FIG. 9.—Plane-polarized photomicrographs of blue-stained thin sections, showing a notable enhancement of the porosity, as evidenced by oversized pores and floating grains in white sandstones (B) compared with the unaltered red ones (A).

abundance of the carbonate cement (Table 3). The detrital mineralogy has little regional variation and typically includes 43 vol. % lithic fragments (L), 29 vol. % mono- and polycrystalline quartz (Q), and 28 vol. % feldspar (F) with plagioclase (P) >> K-feldspar (FK) (Table 3). Accessory minerals include martite (hematite pseudomorphs after magnetite), micas, tourmaline, zircon, and rutile. Lithic fragments comprise mainly volcanic detritus (basaltic, andesitic, felsitic, and vitreous) and subordinate plutonic, sedimentary, and metamorphic grains. Previous to their erosion or the deposition of sediments, most of the volcanogenic protoliths were partially replaced by chlorite and illite. Host-clast mineralogy reveal that: a) mesosilicic and basic volcanic grains are altered to chlorite and b) feldspars and felsitic and vitreous volcanic grains are altered to illite.

Diagenetic Facies
Facies Description

Four diagenetic facies are revealed in colorful exposures of the Huincul Formation: red, gray, brown, and white. Regionally, the red (grayish red 5R 4/2–10R 4/2) and the white sandstones (white to very pale gray N9–N8) are the most widespread, whereas the gray (medium light gray N6

and the brown sandstones (dusky yellow to light olive brown 5Y 6/4–5Y 5/6) are at the contact between the previous ones (i.e., red and white) (Fig. 4A). The visual distinctions are created by characteristic diagenetic variations in cements and grain coatings.

The red sandstones show finely dispersed red hematite grain coatings, even between grain contact points (Fig. 6A). Hematite also fills pore spaces and replaces detrital magnetite and basic to mesosilicic volcanic fragments. Pore-filling kaolinite occurs as aggregates of euhedral crystals, typically forming books of stacked flakes with pseudo- hexagonal shapes (Figs. 6B, 7A). Infrared data and chemical analysis reveal well-ordered kaolinite, which does not contain abundant iron (< 0.05 wt. %) in its structure (Fig. 8A, B). Detrital quartz and feldspar grains are cemented by euhedral, syntaxial quartz (2 vol. %) and albite (0.5 vol. %; Ab_{99}), respectively (Tables 3, 4). Albite overgrowths may have different mineral chemistry and crystallography than the substrate grains, leading to an absence of optical continuity (i.e., non-uniform optical extinction positions) (Worden and Burley 2003). The overgrowths cover the hematite grain coatings (Fig. 6A, C). The well-developed euhedral quartz overgrowths suggest that they were precipitated very early, after the formation of hematite grain coatings but prior to compaction. Two types of carbonate cement are evident: a) non-ferroan calcite in sharp contact with quartz overgrowths (Fig. 6D) and b) minor ferroan calcite that replaces grains and overgrowths (Fig. 6E). Some grains have been completely replaced by carbonate, but their contours are marked by hematite rims. Occasionally, clusters of titanium oxide, calcium, and barium sulfate (gypsum/anhydrite and barite) cements fill pores. Porosity (up to ~ 12%; Fig. 9A) varies as a function of the degree of carbonate cementation (Table 3).

In the white sandstones, red hematite is present only in minor amounts, commonly underlying the quartz and albite overgrowths (Fig. 6F, G); it can be also as coarse-grained hematite in lithic fragments and detrital, martitized magnetite. In some cases, hematite coatings do not occur between detrital grains and overgrowths, suggesting that it was never present. Dissolution features include vugs in quartz overgrowths (Fig. 6F) and ragged edges of the kaolinite plates (Fig. 7B). Similarities in infrared data suggest that the kaolinite in the bleached sandstones belongs to the same unique early burial event of kaolinite precipitation (Fig. 8C). Feldspar and volcanic grains are altered strongly to smectite, which also occurs as rims of crenulated plates. Smectite postdates and replaces the early authigenic pore-filling kaolinite (Fig. 7B). Albite overgrowths (Figs. 6G, 7B) and detrital K-feldspar (orthoclase) are rather well preserved. White sandstone shows a pronounced development of secondary porosity (~ 23%, Table 3), with oversized pores and floating detrital grains (Fig. 9B). The late poikilotopic calcite includes isolated corroded detrital grains, suggesting that it precipitated after pervasive clast dissolution. This late calcite precipitation may reduce secondary porosity to almost zero. A striking feature of the poikilotopic calcite is the presence of abundant primary hydrocarbon-bearing fluid inclusions. Bitumen occurs at the boundary between crystals of the calcite cement, as impregnations of detrital grains, and fills microfractures in clasts (Fig. 6H), attesting to the former presence of liquid hydrocarbons in the pore space (Littke et al. 1990). In addition to bitumen impregnations, pipes and tubes of hydrocarbons and silicified logs (up to 12 m long) are abundant in the upper bleached level (Fig. 5).

In the gray sandstones, the smectite is much more abundant based on the XRD difractogram intensities, and its composition is close to that of a montmorillonite with small amounts of copper (Fig. 10). The montmorillonite commonly is associated with minor amounts of chlorite–montmorillonite mixed-layer minerals containing minor amounts of Cu and V and microgranular euhedral quartz (Fig. 7C). Where interstratified chlorite–smectite predominates, sandstones turn to tan hue, defining the brown facies (Fig. 6I). Secondary V-bearing hematite with a typical rosette arrangement is associated with the montmorillonite (Fig. 7D).
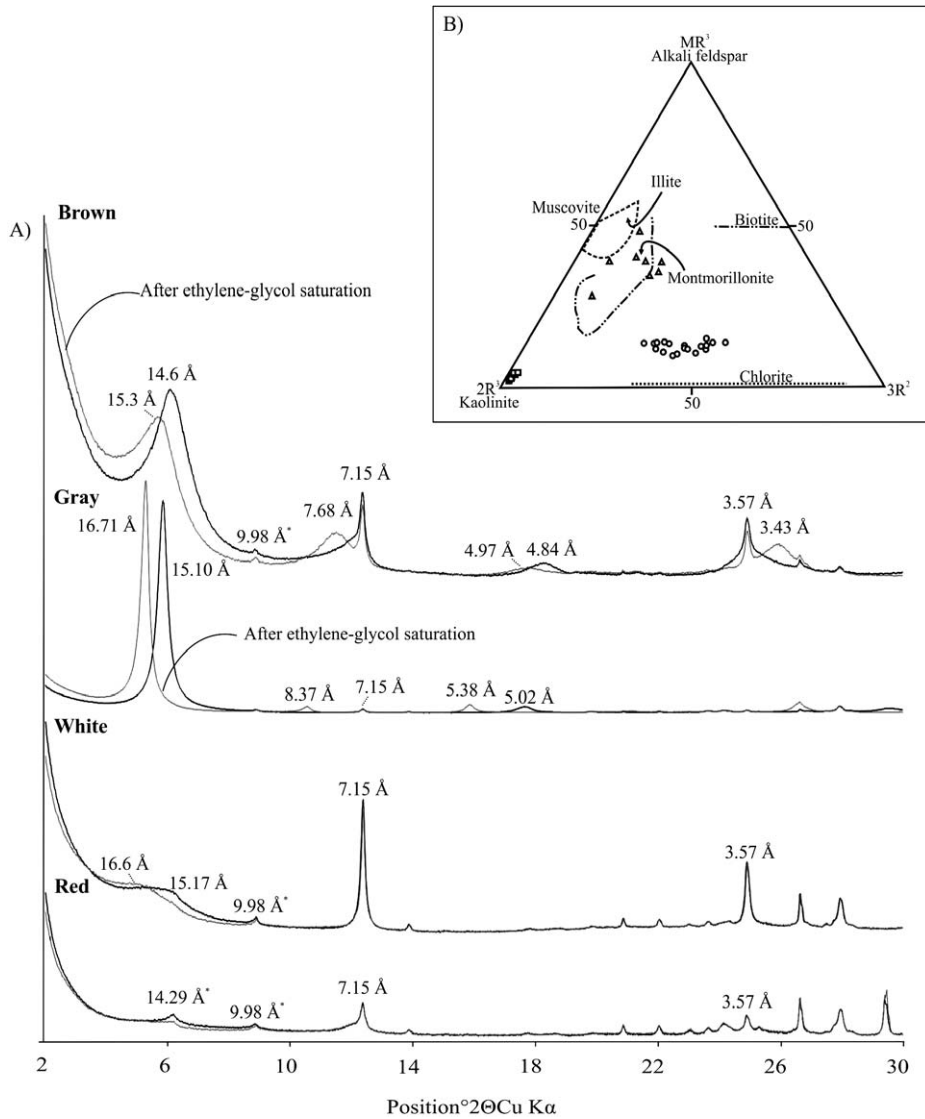
FIG. 10.—**A)** X-ray diffraction patterns for red, white, gray, and brown sandstones. Black = air dried, gray = glycolated. Main *d* values of dominant minerals are listed. The occurrence of kaolinite is recorded in all diagenetic facies, whereas smectite is present in the white facies but predominates in gray sandstones; less shifting after ethylene glycol in brown sandstones indicates chlorite–smectite mixed-layer mineral. Inherited chlorite and illite are commonly present (*d* values are indicated with *). Intensities of red, white, and brown sandstones have been increased by a factor of 7 in order to compare them with the gray sandstones, due to their lower clay content. **B)** Plot of the clay-mineral composition in the MR^3-$2R^3$-$3R^2$ triangle in which silica is considered as a component in excess, $MR^3 = Na + K + 2Ca$; $2R^3 = ((Al + Fe^{3+}) - MR^3)/2$, and $3R^2 = (Mg + Mn + Fe^{2+})/3$ (Velde 1985). Smectite composition from the gray facies plot in the montmorillonite field (triangles), whereas the mixed-layer chlorite–smectite (brown facies) plot between the montmorillonite and chlorite compositions (squares).

Bitumen occurs as random impregnations of detrital grains. Relics of calcite cement are rare. The porosity has been enhanced (Table 3) by the dissolution of clasts and cements.

In the bleached sandstones, volcanic and volcaniclastic grains show pseudoductile deformation and some quartz and feldspar grains have numerous brittle microfractures. These features have also been observed in the brown and gray sandstones, but they have less intensity.

Major-Element and Trace-Element Distribution

Chemical data from vertical transition from the red to the bleached sandstones through intermediate gray and brown facies shows variations in both major oxides and trace elements (Table 1; Fig. 11). The major-element distributions in the unaltered red sandstones and altered white, gray, and brown sandstones are illustrated in Harker-type diagrams with Al_2O_3, Fe_2O_3, K_2O, Na_2O, MgO, TiO_2, FeO, MnO, and Zr plotted against SiO_2 (Fig. 11A). The distribution of the trace elements V, Cu, and U was outlined in each stratigraphic profile (Fig. 11B). CaO was not considered, due to its sensitivity to the highly variable carbonate cement content, which could lead to misinterpretations of the behavior of this oxide during the alteration. In the white sandstones, the concentrations

of Al_2O_3, Fe_2O_3, Na_2O, and TiO_2 are lower than in the red sandstones (Fig. 11A). MgO and FeO show similar behavior, except for the enrichment exhibited by two samples that contain more smectite. MnO is enriched in the white sandstones, with the exception of the two samples that contain high FeO. In the gray sandstones Al_2O_3, Fe_2O_3, Na_2O, and TiO_2 behave as in the red sandstones, whereas in the brown sandstones these oxides show concentrations similar to those of the white facies. The MgO and FeO enrichment exhibited by these facies (gray and brown) is coincident with the presence of montmorillonite and chlorite–montmorillonite, and this enrichment is higher in the brown facies, which contains more chlorite–montmorillonite than montmorillonite. In the red and gray facies, the Zr values are higher than in the white and brown facies, except for two samples that show contrasting behavior. K_2O becomes enriched as the SiO_2 content of sandstones increases, but does not show different behavior between red beds and altered facies. The lower amount of these oxides belongs to samples with higher carbonate cement content, indicating that the concentration of K_2O and SiO_2 are mainly related to the amount of silicates (detrital grains) in the sandstone and were not affected by the alteration process. In both profiles, gains of V were recorded only in the gray facies, whereas Cu gains have been identified in all the altered sandstones (i.e.,
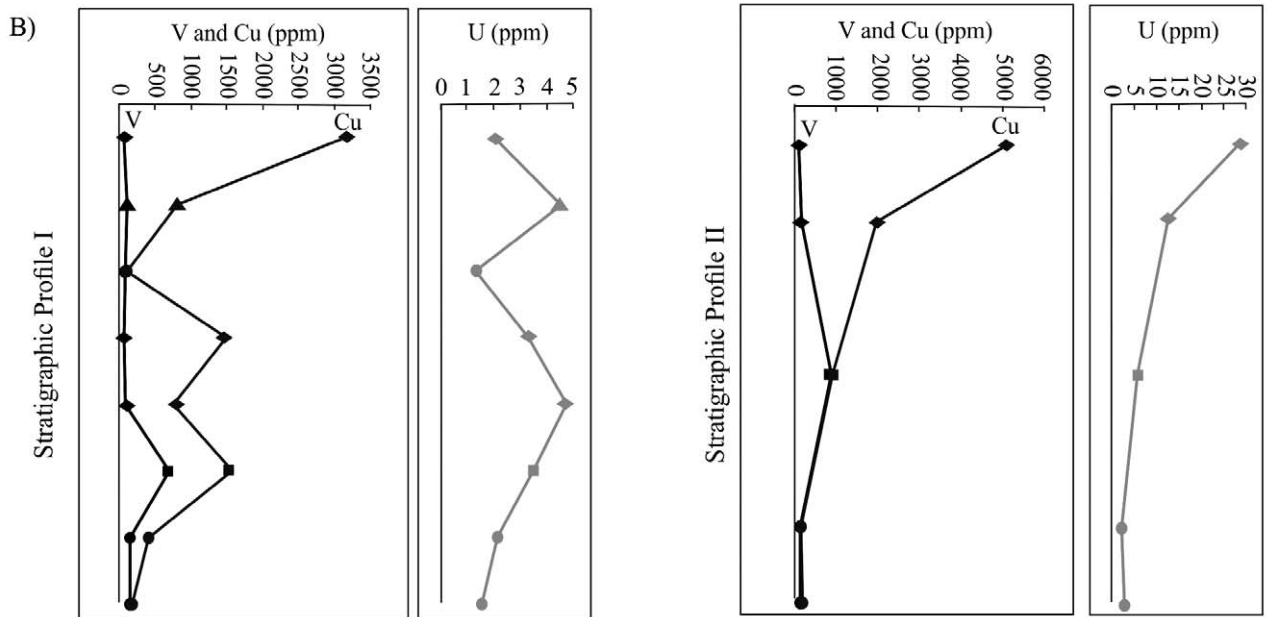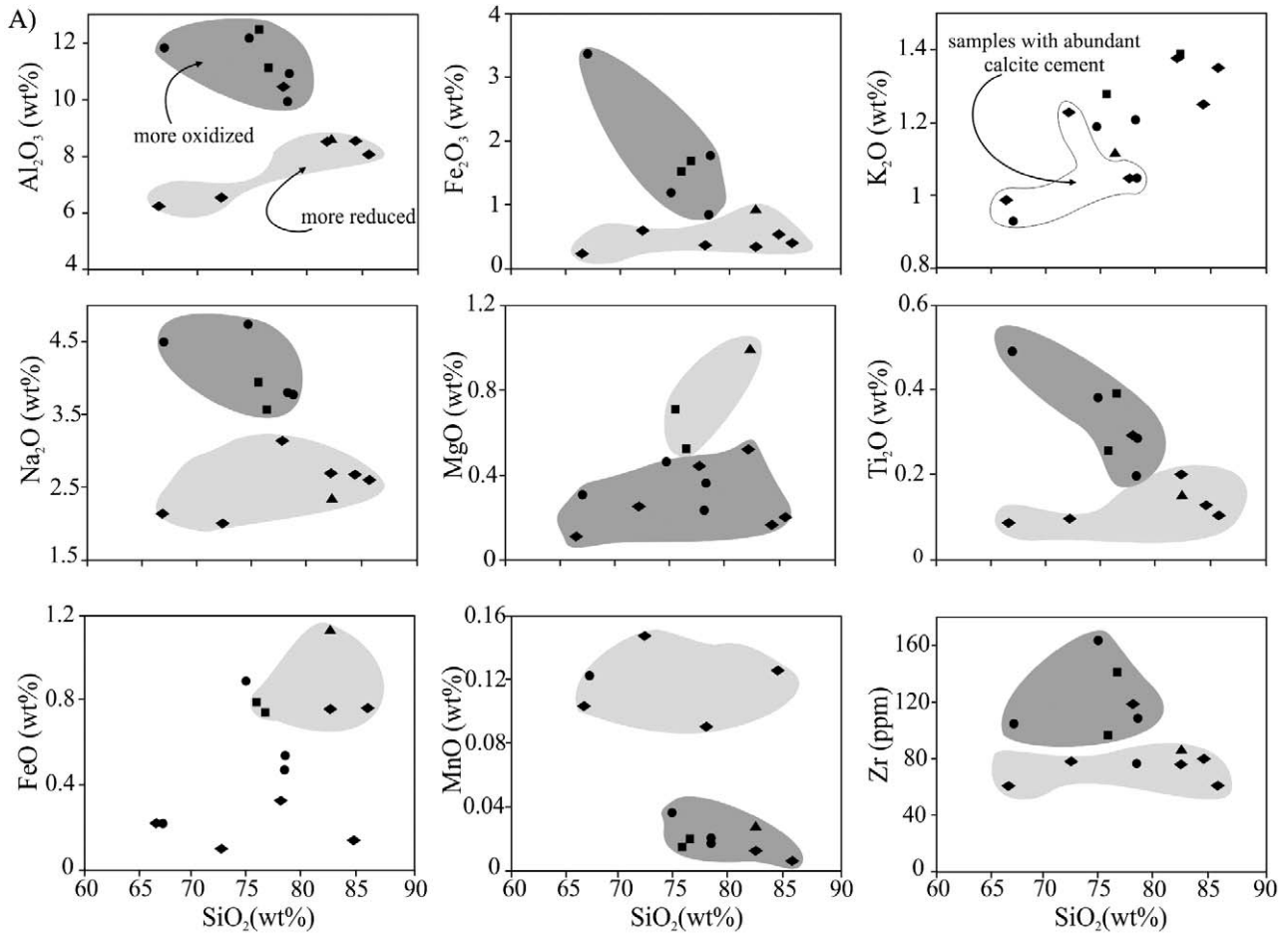
FIG. 11.—Distribution of major, minor, and trace elements. A) Harker-type diagrams for major and minor elements. Light and dark fields include reduced and oxidizing diagenetic facies, respectively. B) V, Cu, and U concentrations and their distribution in stratigraphic profiles I and II.
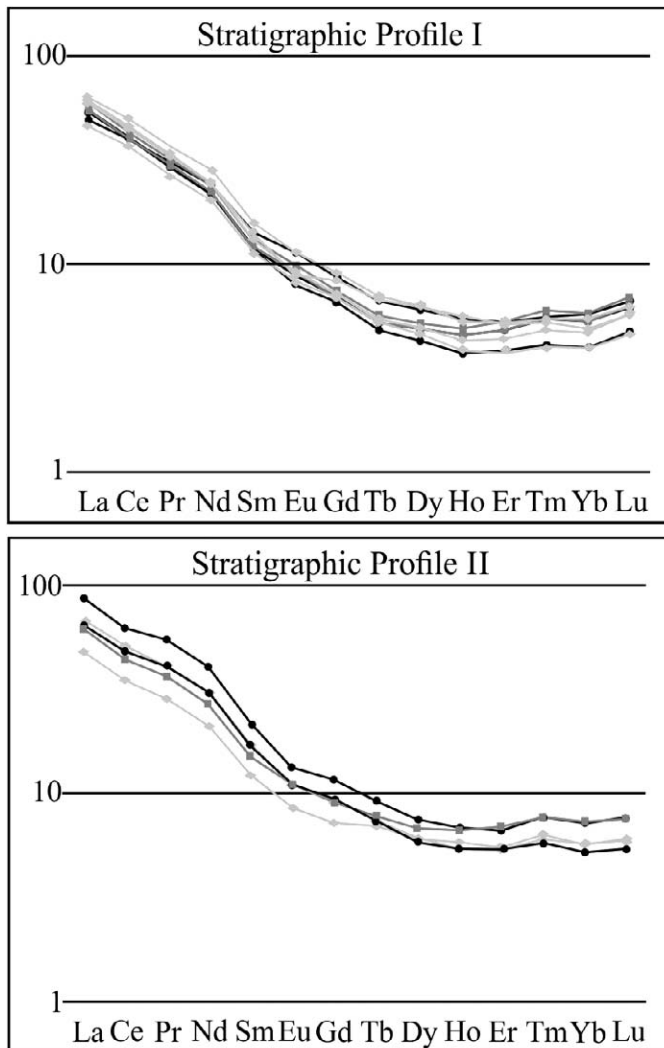
Fig. 12.—Chondrite-normalized REE diagrams (Boynton 1984) for the diagenetic facies of both profiles.

white, gray, and brown) (Fig. 11B). U also shows gains, especially in the white facies of the second profile, but the net concentration of this element is very low (Fig. 11B).

DISCUSSION

Color variations within the Huincul Formation evident in satellite imagery are correlated with textural, mineralogical, and chemical differences in sandstone from two stratigraphic profiles. Based on these differences, four facies were defined: red, gray, brown, and white. The paragenetic sequence indicates a complex stage of alteration (bleaching) controlled by fluid–rock interaction. The absence of hematite in the bleached horizons of the Huincul Formation is not depositionally controlled. This interpretation is evident from relics of hematite preserved beneath quartz and albite overgrowths in these bleached horizons, which

protected Fe oxides from pore fluids and thus inhibited further mineral reactions. Only a few white sandstones appear to have never been red, probably related to the presence of localized organic matter (e.g., tree trunks). The presence of organic matter in the Huincul Formation is likely random, however, and could not explain the regional decoloration in the study area. The reduction of iron oxides is interpreted to have resulted from the interaction between the host rocks and one or more extraformational fluids. Although hydrocarbons, organic acids, methane, and hydrogen sulfide are all capable of causing the reduction (Elmore et al. 1989; Lee and Bethke 1994; Rowe and Burley 1997; Garden et al. 2001; Beitler et al. 2005), several lines of evidence favor interpretation that the presence of hydrocarbon fluids within the LCh at the time of reduction. These observations include bitumen impregnations, pipes and tubes of hydrocarbons, and hydrocarbon-bearing fluid inclusions. The distribution of reduction patterns (at the top of the sedimentary succession) indicates that the fluids responsible for the reduction were buoyant and immiscible with the connate waters. Thereby, the red facies represents unaltered deposits, and the white facies represent the sandstones modified by hydrocarbon influx. The gray and the brown facies are interpreted to be a consequence of the interaction between reducing and oxidizing fluids at the redox front.

Variations in major oxides and trace elements among sandstones facies (Table 1; Fig. 11) are interpreted to depend on the degree of interaction with hydrocarbon-bearing solutions. This assumption is supported by the constant pattern of the REE (Fig. 12), which indicates that the general type of igneous rock debris dominant in the detritus is the same in all diagenetic facies (Fralick 2003). Moreover, REE are unaffected by diagenesis (Chaudhuri and Culers 1979 in Fleet 1984) and its constant pattern reflects detritus provenance and not any diagenetic changes.

Tectonic Control on the Stratigraphic Evolution of the Huincul Formation: Relationship with Fluid-Flow Pathways

The stratigraphic succession in the Huincul Formation was deposited by meandering rivers. Channel deposits show obvious point bars and extensive lateral accretion. The organization of the facies association resulted from tectonic stages developed in the evolution of the foreland basin (Rainoldi et al. 2012b), related to contractional deformation in the Agrio fold-and-thrust belt to the west (Ramos and Kay 2006). During tectonic quiescence, sediment supply was balanced with subsidence, giving a characteristic meandering sequence with channel, point-bar, and floodplain development. This scenario is reflected near the base of the stratigraphic profiles, where high subsidence rate is interpreted to drive high A/S (accommodation/supply), favoring the development of channels dominated by lateral migration and associated floodplains (Fig. 4A, B). This situation favored the deposition of isolated permeable strata (e.g., channels) and preserved the red beds from bleaching. On the other hand, toward the top of the succession, low subsidence rate is interpreted to be dominated by low A/S, favoring extensive lateral accretion, vertically stacked channels, and the starvation of the floodplain, whose remnants are present as muddy clasts at the bases of the cycles (Fig. 4D, E) (Rainoldi et al. 2012b). Interconnection among permeable channel strata facilitated the migration of the reducing fluids, leading to decoloration, resulting in the development of the bleached sandstones.

Diagenetic Features Related to Burial History in Oxidizing Conditions (Eogenesis to Mesogenesis)

Red-Bed Facies.—The presence of red coatings at the grain-to-grain contact point indicates early precipitation of hematite (Beitler et al. 2005). Thus, reddening of the sandstones may have been developed under eodiagenetic conditions, as infiltration of oxidizing and slightly acidic
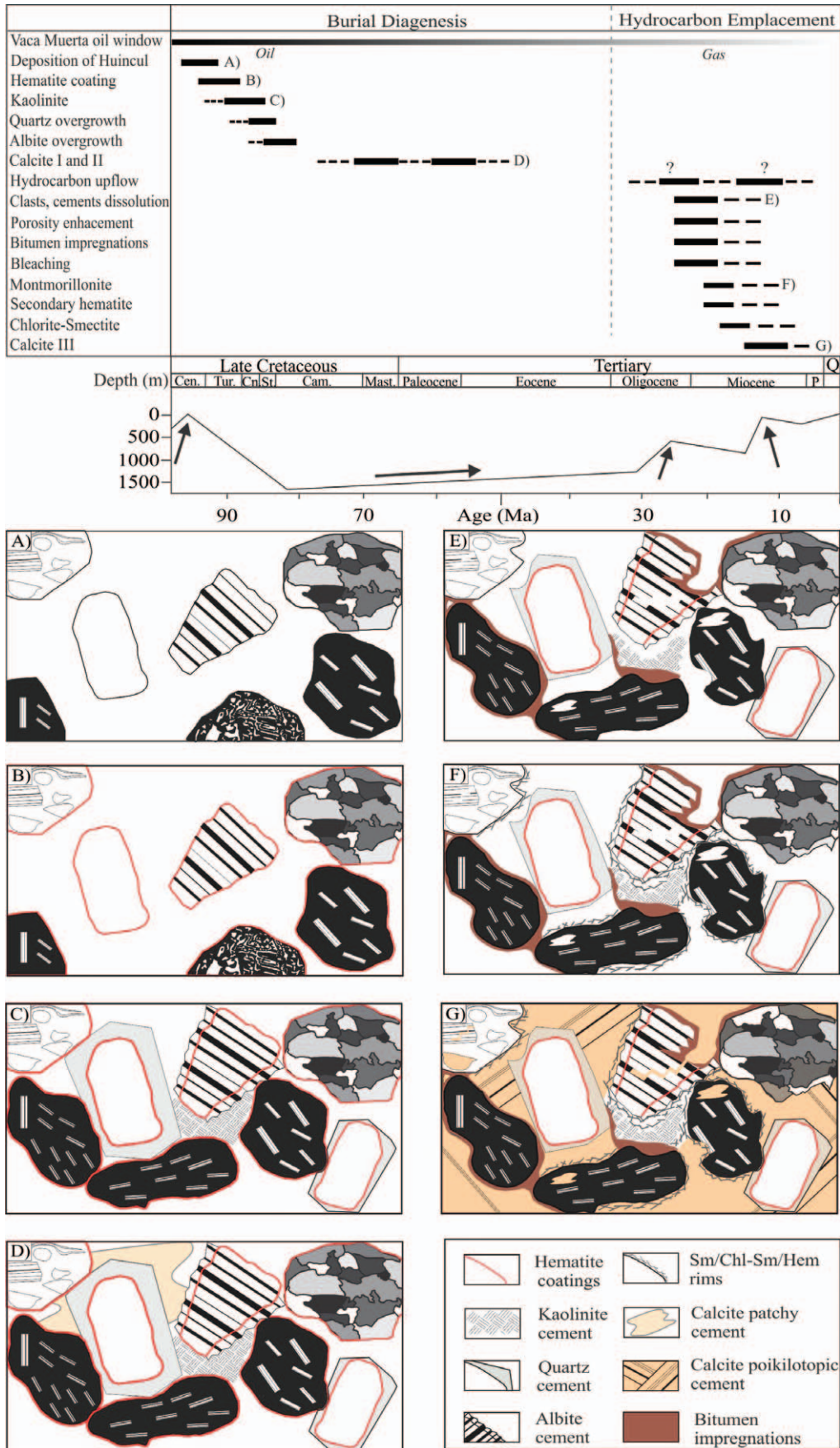
meteoric water (Brown 2005) produced the breakdown of ferrous iron-rich oxides (e.g., magnetite) and silicate minerals (Walker 1989). Oxidizing agents must have been consumed by the production of hematite (Reaction 1; Langmuir 1997; Iron is redeposited as iron hydroxide followed by the crystallization to hematite, Brown 2005) (Fig. 11):

$$Fe^{2+} + \tfrac{1}{4}O_2 + \tfrac{5}{2}H_2O = Fe(OH)_3 + 2H^+ \tag{1}$$
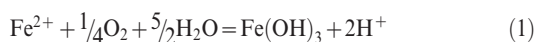
Kaolinite in the red beds may have precipitated under acidic conditions related to the migration of dilute freshwater into the sediment. The absence of dickite in the kaolin is indicative of crystallization at a relatively shallow burial depth, which never reached 2.5 to 3 km in case of normal geothermal gradient (Lanson et al. 1995; Beaufort et al. 1998).

Subsequent compaction and circulation of formation waters enriched in silica and sodium may have favored the precipitation of quartz and albite overgrowths. Early quartz overgrowths are interpreted to indicate relatively shallow conditions during the sandstone burial (Fig. 13), possibly near the eogenesis–mesodiagenesis transition. In many cases, these stages are favorable for the first episodes of silica precipitation (Scasso and Limarino 1997 and references therein) at temperatures above 70°C (McBride 1989; Bjørlykke and Egeberg 1993; Worden and Morad 2000) and depths of 1–2 km (Bjørlykke and Egeberg 1993, and references therein). The overgrowths of albite suggest that the pore fluid was enriched in sodium due to dissolution of previous Na-rich minerals such as detrital volcanic glass or early diagenetic analcite. This last mineral is more evident in sandstones of the Huincul Formation in the areas near the margin of the basin. The overgrowths of albite indicate an increase in the temperature of the system, considering that albitization in a sedimentary environment is mainly due to a mesogenetic burial process (temperatures above 90°C) (Hirt et al. 1993; Yu et al. 1997; Ehrenberg and Jakobsen 2003; González-Acebrón et al. 2010). Oxidizing and low-P_{CO2} conditions may have prevailed, precipitating non-ferrous calcite in pore spaces (Fig. 13).

Late ferrous calcite cement replaced clast overgrowths and clastic fragments, indicating a decrease in the Eh conditions, probably during mesodiagenesis. Maximum burial diagenesis for the Huincul Formation in Los Chihuidos was estimated around early to middle mesodiagenesis (Rainoldi et al. 2012a). Taking into account the open grain packing, significant porosity (Fig. 9A), and the relatively shallow burial history (only 2000 m burial depth) of the Huincul Formation, it follows that the effects of compaction were not intense and permeability and porosity could have been easily preserved with burial. This situation may have favored the circulation of hydrocarbons and related fluids, as suggested by the bleaching of red sandstones and the impregnations of bitumen in the bleached facies.
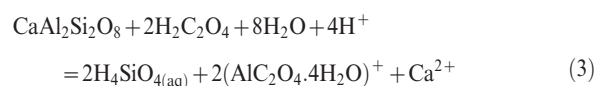
Diagenetic History Related to Fault-Controlled Migration of Hydrocarbons

White Facies.—In the white facies, hematite coatings have been dissolved, resulting in the red bed decoloration (i.e., bleaching). In addition to the hematite dissolution, the carbonate cement, some (scarce) quartz overgrowths, and volcanic and feldspar clasts were partially dissolved and feldspar and vulcanite grains were pervasively altered (Fig. 13). Therefore, the most prominent characteristic of the white

samples is the creation of the secondary porosity. Locally, however, the early silicification of tree trunks in the upper strata may have generated abundant organic acids that inhibited the development of oxidizing conditions during diagenesis, and these were never oxidized.

The influx of formation waters carrying hydrocarbons and other organic and inorganic species in a water-wet system (i.e., organic acids, methane, and CO_2; Carothers and Kharaka 1978) into the red sandstones may have induced a change in the geochemical conditions, making pore fluids more reduced. Organic acids, in particular, may have promoted the dissolution of aluminosilicates and carbonates of the red beds (Surdam et al. 1984, 1989) (reactions 2 and 3; modified from Surdam et al. 1984) (Fig. 13). Oversized pores (Fig. 9B) imply that destruction of feldspars or unstable rock fragments have been extensive. Depending on the source of organic acids, two possible situations may have taken place: 1) organic acids were produced by biodegradation of hydrocarbons in the sandstones (the microbial metabolism of petroleum to generate heavy oils, CO_2, organic acids, and other intermediates; Larter et al. 2006), a process that occurs under anaerobic conditions at temperatures below 80°C, or 2) organic acids travelled together with hydrocarbons diluted in the formation waters until they reached the sandstones with a temperature between 80° and 120°C, the range of temperatures at which organic acids reach the peak of concentration (Carothers and Kharaka 1978).

In addition to their effect on aluminum mobility, carboxylic acids can also dissolve quartz (Surdam et al. 1984) at pH near 6.7, but its capacity of dissolution decreases sharply at lower pH (Bennett and Siegel 1987; Bennett et al. 1988). Thus, at a pH near 6 (a common pH for hydrocarbon reservoirs, e.g., Surdam et al. 1989), only scarce quartz dissolution could have taken place (Fig. 13). In these conditions, low-temperature albite overgrowths would not be affected by alteration, due to their greater stability compared to clastic high-temperature feldspars of intermediate composition (Pittman 1979). Detrital K-feldspar may also persist under the conditions where biodegradation took place (Ehrenberg and Jakobsen 2003).

$$CH_3COOH + CaCO_3 = CH_3COO^- + Ca^{2+} + HCO_3^- \tag{2}$$

$$CaAl_2Si_2O_8 + 2H_2C_2O_4 + 8H_2O + 4H^+$$
$$= 2H_4SiO_{4(aq)} + 2(AlC_2O_4 \cdot 4H_2O)^+ + Ca^{2+} \tag{3}$$

Redox reactions of hydrocarbons and organic acids (reaction 4, modified from Surdam et al. 1993) with oxidized species (e.g., hematite) produced Fe^{2+}_{aq} that was mainly removed from the infiltrated sandstones. Marked losses of Fe_2O_3 (Fig. 11A) correspond to removal of hematite grain coatings. At the same time, the organic reductant was oxidized. The lack of pyrite was probably due to the absence of sulfide concentrations in the reducing pore waters.

$$C_9H_{20} + 4Fe_2O_3 + 3CO_2 + 16H^+ = 6CH_3COOH + 8Fe^{2+} + 6H_2O \tag{4}$$
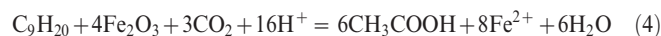
The dissolution of detrital clasts and early cements led to elemental transport of Al_2O_3, Na_2O, MgO, and FeO (Fe^{3+} reduced to Fe^{2+}) (Fig. 11A) in solution due to their complexation with organic anions and

←

FIG. 13.—Paragenetic sequence and burial history of the Huincul Formation. Arrows in the burial diagram indicates the episodes of uplift (after Zamora Valcarce et al. 2009). Relative timing of oil emplacement and related sandstone recorded alteration, which may have taken place during one of the two stages of uplift registered in the Tertiary. In the figures, some detrital grains and cements have been magnified in order to show all the identified processes.

later precipitation at the redox front (and locally in the reducing compartment). Dissolution and redox reactions (reaction 2) generated CO_2 as a by-product, increasing the P_{CO2}. As the alkalinity was externally buffered by carboxylic acids, the increase of the P_{CO2} may have favored the precipitation of late carbonate cement (Surdam et al. 1984, 1989). Mobile behavior of TiO_2 (Fig. 11A) can be attributed to the presence of organic acids, which can form chelation complexes with Ti^{4+} (Salmien et al. 2005), whereas the higher concentrations of MnO (or FeO; Fig. 11A) are interpreted as an indicator of high reducing conditions in the white sandstones.

Intermediate Facies Developed in the Redox Front.—Hydrocarbon-bearing solutions responsible for the bleaching of sandstones reached intermediate redox conditions at the contact zone with the red beds. Metastable geochemical conditions between red and white rocks resulted in the gray and minor brown sandstones where secondary montmorillonite and hematite may coexist with chlorite–smectite mixed layers. The presence of chlorite–smectite mixed-layer minerals and secondary hematite is indicative of different redox conditions (more reducing and more oxidizing conditions, respectively). The present association of both reduced and oxidized minerals suggests temporal changes in the Eh conditions probably related to fluctuations in the location of the redox front. These changes may have favored the destabilization of the soluble Al–organic complex generated during the dissolution of silicates in the altered sandstones (Reaction 3), precipitating the highest amount of smectite (montmorillonite) with interstratified chlorite–smectite along the boundary zone, evident in the gains of MgO and FeO (Fig. 11A). Nevertheless, the high concentration of MgO in both intermediate facies cannot be explained by MgO losses of the red sandstones (Fig. 11A), suggesting that the altered fluid may have been enriched in this element. Excess of silica was precipitated in microquartz clusters.

If primary hematite has been leached, the high Fe_2O_3 wt. % in the gray facies (Table. 1; Fig. 11A) is due to the precipitation of secondary V-bearing hematite. The gray facies has a chemical composition similar to the red sandstones, whereas the composition of the brown facies is similar to that of the white sandstones (Fig. 11A). Thus, the gray and brown facies represent more oxidizing and reducing conditions, respectively, at the redox front.

The presence of V and Cu in most of the secondary minerals of the grey and brown facies enhances the role of the redox front in the precipitation of metallic elements, for which speciation is very sensitive to Eh conditions. Copper may have been transported by chloride-rich formation waters, whereas V could have been carried as V^{3+} by the incoming reduced fluids complexed with dissolved organic matter (Granger, oral communication, 1983 in Goldhaber et al. 1990). V-bearing chlorite or chlorite–smectite mixed layers have been reported to be indicative of the redox fronts in the V-U deposits of the Henry Basin, Utah, in the United States (Goldhaber et al. 1990; Northrop et al. 1990). The occurrence of vanadium in petroleum-related fluids has been observed previously in bitumen from the Vaca Muerta Formation (Parnell and Carey 1995) and worldwide in oil fields, and bitumen and asphalt deposits (DeGolyer 1924 and references therein; Breit and Wanti 1991; Parnell and Carey 1995).

The relative paucity of calcite in the redox front may be related to the precipitation of abundant smectite and interstratified chlorite–smectite, which decreased the pH by removing the hydroxide ion from solution to form $MgO(OH)_2$ and $Fe(OH)_2$. Cu and V may have contributed to lowering the pH in case they occupied the octahedral sites of clay minerals $(Cu(OH)_2, V(OH)_3)$ (Goldhaber et al. 1990).

Timing and Migration of Paleo–Fluid Flow in the Huincul Sandstone

By the time the Neuquén Group was deposited, the Vaca Muerta Formation was in the oil window and hydrocarbons could have migrated by vertical faults from the Vaca Muerta to the Mulichinco Formation, the main gas reservoir of the Los Chihuidos high (Aguada Pichana, Sierra Chata, and Parva Negra fields). During the uplift of the Chihuidos block, mainly in the Tertiary (20–25 Ma, and at 14 Ma; Zamora Valcarce et al. 2009), hydrocarbons likely migrated vertically, directly from the source rocks or from the Mulichinco deep reservoir up to the Huincul Formation, to be sealed by the overlying mudstones of Lisandro Formation. The north–south trending reverse faults of the LCh, which are detached from the Auquilco Formation (Bringworth et al. 2011), must have been the channels for the migration of hydrocarbons. These faults in some cases reached the sandy levels of the Mulichinco Formation, but sometimes they propagated upward to surface levels (Bringworth et al. 2011). Other deeper structures comprise normal faults that affect the deposits of Lotena Formation and several Pre-Cuyo half-graben structures, some of which show evidence of tectonic inversion (Bringworth et al. 2011). Furthermore, 2D seismic data indicates that hydrocarbon seepage occurred in LCh during the late Oligocene and Miocene (Giusiano et al. in press). Evidence for basin-wide secondary migration into the carrier-bed sandstones is evident in the satellite image by a north–south alteration front and its dissipation to the east (Fig. 2C, D), features that suggest an eastward migration of the hydrocarbon-bearing solutions. Fluid flow could migrate laterally into the sandstone where fluids were stratified, hosting hydrocarbons in the upper part and water in the lower part of the reservoir due to the buoyancy of hydrocarbons, resulting in the typical water–hydrocarbon contact (Rainoldi et al. 2012a). However, in the outcrops the pathway of oil migration through the sandstones seems rather tortuous in three dimensions, due, in part, to permeability heterogeneity as well as formation water dynamics (Rhea et al. 1994).

CONCLUSIONS

The Huincul Formation (late Cenomanian–early Turonian) at LCh was deposited in a foreland basin related to the contractional deformation of the Agrio fold-and-thrust belt to the west. During uplifting stages, low accommodation space and higher supply of sediments gave rise to the amalgamation of fluvial channels, providing well connected highly permeable strata where hydrocarbons and related fluids could later easily flow. During deposition of the Upper Cretaceous Neuquén Group, the Vaca Muerta Formation source had already started to generate hydrocarbons, which migrated to the Mulichinco Formation. During Huincul Formation deposition, infiltration of meteoric waters of oxidizing and slightly acidic conditions generated sandstones reddening at eogenetic conditions. The maximum burial for this formation was calculated < 2 km.

Striking color variations in the Huincul Formation are attributed to the development of a regional-scale redox system. Field, petrographic, and geochemical analyses discriminate four diagenetic facies, each with a distinct color. Bleaching of red beds related to moderate regional diagenesis is linked to structure-controlled upflow of hydrocarbons and associated fluids, and chemical reactions between reducing fluids and diagenetic minerals.

Tertiary uplift and reactivation of deep faults must have induced the rupture of the Mulichinco reservoir, releasing hydrocarbons, or favoring the expulsion of hydrocarbons directly from the source into the Huincul Formation. Once in the sandstones, iron was reduced to Fe^{2+} due to redox reactions of hematite with hydrocarbons and related organic-matter-rich water. Clasts and cement were partially dissolved, resulting in the bleaching of the original red beds. Authigenic Cu-bearing smectite and Cu-V-bearing mixed-layer chlorite–smectite with secondary V-bearing hematite precipitated in the gray and brown facies in response to the reactions between the oxidized and reduced fluids at the redox front. Sandstones within the redox interval contain more magnesium than the unaltered red beds, indicating the influx of magnesium-rich fluids.

During the subsequent uplift stages, denudation reached the mudstones of the overlying Lisandro Formation, which had acted as a regional seal for the sandstones. Consequently, the erosion generated the exhumation and exposition of the Huincul reservoir, resulting in the ultimate release of the hydrocarbons.

This multi-scale investigation of diagenetic features related to burial history and to structure-controlled upflow of hydrocarbons in a succession of siliciclastic rocks enhance modeling of a regional-scale redox system worldwide. Our study offers new insight into the application of authigenic minerals to trace hydrocarbon pathways along red beds and to evaluate the reservoir quality, in understanding the importance of fluid compositions, mixing, and fluid–rock interaction along a major redox system.

REFERENCES

ANECHINE, M., STAHLSHMIDT, E., AND DEL PINO, M., 2002, Evaluación petrofísica de reservorios complejos dentro de la Formación Mulichinco. Yacimiento Sierra Chata. Cuenca Neuquina: V Congreso de Exploración y Desarrollo de Hidrocarburos V, CD-ROM, 10 p.

ARDOLINO, A., AND FRANCHI, M., 1996, Geología y Recursos Naturales del Departamento de Añelo, provincia del Neuquén, República Argentina: Dirección Nacional del Servicio Geológico, Anales 25, p. 1–212.

BEAUFORT, D., CASSAGNABERE, A., PETIT, S., LANSON, B., BERGER, G., LACHARPAGNE, J.C., AND JOHANSEN, H., 1998, Kaolinite to dickite reaction in sandstone reservoirs: Clay Minerals, v. 33, p. 297–316.

BEITLER, B., PARRY, W.T., AND CHAN, M.A., 2003, Bleaching of Jurassic Navajo Sandstone on Colorado Plateau Laramide highs: evidence of exhumed hydrocarbon supergiants?: Geology, v. 31, p. 1041–1044.

BEITLER, B., PARRY, W.T., AND CHAN, M.A., 2005, Fingerprints of fluid flow: chemical diagenetic history of the Jurassic Navajo Sandstone, southern Utah: Journal of Sedimentary Research, v. 75, p. 457–561.

BENNETT, P., AND SIEGEL, D.I., 1987, Increased solubility of quartz in water due to complexation by dissolved organic compounds: Nature, v. 326, p. 684–687.

BENNETT, P.C., MELCER, M.E., SIEGEL, D.I., AND HASSETT, J.P., 1988, The dissolution of quartz in dilute aqueous solutions of organic acids at 25°C: Geochimica et Cosmochimica Acta, v. 52, p. 1521–1530.

BENSING, J.P., MOZLEY, P.S., AND DUNBAR, N.W., 2005, Importance of clay in iron transport and sediment reddening: evidence from reduction features of the Abo Formation, New Mexico, U.S.A.: Journal of Sedimentary Research, v. 75, p. 562–571.

BJØRLYKKE, K., AND EGEBERG, P.K., 1993, Quartz cementation in sedimentary basins: American Association of Petroleum Geologists, Bulletin, v. 77, p. 1536–1548.

BOYNTON, W.V., 1984, Cosmochemistry of the rare earth elements: meteoritic studies, in Henderson, P., ed., Rare Earth Element Geochemistry: Amsterdam, Elsevier, p. 63–114.

BREIT, G.N., AND WANTY, R.B., 1991, Vanadium accumulation in carbonaceous rocks: a review of geochemical controls during deposition and diagenesis: Chemical Geology, v. 91, p. 83–97.

BRINGWORTH, W., POSE, F.A., AND GANGUI, A., 2011, Rasgos estructurales del subsuelo en el área de Aguada Pichana, provincia de Neuquén, Argentina, in Stinco, L.P., eds., Trabajos Técnicos: VIII Congreso de Exploración y Desarrollo de Hidrocarburos, p. 619–628.

BROWN, A.C., 2005, Refinements for footwall red-bed diagenesis in the sediment hosted stratiform copper deposits model: Economic Geology, v. 100, p. 765–771.

CAROTHERS, W.W., AND KHARAKA, Y.K., 1978, Aliphatic acid anions in oil-field waters: implications for origin of natural gas: American Association of Petroleum Geologists, Bulletin, v. 62, p. 2441–2453.

CAZAU, L., AND ULIANA, M.A., 1973, El Cretácico superior continental de la Cuenca Neuquina: V Congreso Geológico Argentino, v. 3, p. 131–163.

CHAN, M.A., PARRY, W.T., AND BOWMAN, J.R., 2000, Diagenetic hematite and manganese oxides and fault-related fluid flow in Jurassic sandstones, southeastern Utah: American Association of Petroleum Geologists, Bulletin, v. 84, p. 1281–1310.

CHEBLI, G., MENDIBERRI, H., GIUSIANO, A., IBÁÑEZ, G., AND ALONSO, J., 2011, El shale gas en la Provincia del Neuquén, in Stinco, L.P., eds., Trabajos Técnicos: VIII Congreso de Exploración y Desarrollo de Hidrocarburos, p. 669–692.

CORBELLA, H., NOVAS, F.E., APESTEGUÍA, S., AND LEANZA, H.A., 2004, First fission track-age for the dinosaur-bearing Neuquén Group (Upper Cretaceous) Neuquén Basin, Argentina: Museo Argentino de Ciencias Naturales, Revista, v. 6, p. 1–6.

CRISTALLINI, E.O., MARTÍNEZ, J.M., SANCHEZ, E., PERIALE GÓMEZ, S., AND LONCARICH, A., 2005, Evaluación estructural del bloque Bandurria (Provincia del Neuquén, Argentina): Yacimientos Petrolíferos Fiscales, (unpublished), 73 p.

DE FERRARIIS, C., 1968, El Cretácico del norte de la Patagonia: 3° Jornadas Geológicas Argentinas, v. 1, p. 121–144.

DEGOLYER, E., 1924, The occurrence of vanadium and nickel in petroleum: Economic Geology, v. 19, p. 550–558.

EHRENBERG, S.N., AND JAKOBSEN, K.G., 2003, Plagioclase dissolution related to biodegradation of oil in Brent Group sandstones (Middle Jurassic) of Gullfaks Field, northern North Sea, in Burley, S.D., and Worden, R.H., eds., Clastic Diagenesis: Recent and Ancient: International Association of Sedimentologists, Special Publication 4, p. 541–559.

ELMORE, R.D., MCCOLLUM, R., AND ENGEL, M.H., 1989, Evidence for a relationship between hydrocarbon migration and diagenetic magnetic minerals: implications for petroleum exploration: Association of Petroleum Geochemical Exploration, Bulletin, v. 5, p. 1–17.

FLEET, A.J., 1984, Aqueous and sedimentary geochemistry of the rare earth elements, in Henderson, P., ed., Rare Earth Element Geochemistry: Amsterdam, Elsevier, p. 343–369.

FOLK, R.L., ANDREWS, P.B., AND LEWIS, D.W., 1970, Detrital sedimentary rock classification and nomenclature for use in New Zealand: New Zealand Journal of Geology and Geophysics, v. 13, p. 937–968.

FRALICK, P., 2003, Geochemistry of clastic sedimentary rocks: ratio techniques, in Lentz, D.R., ed., Geochemistry of Sediments and Sedimentary Rocks: Evolutionary Considerations to Mineral Deposit-Forming Environments: Geological Association of Canada, Geotext 4, p. 85–103.

GARDEN, I.R., GUSCOTT, S.C., BURLEY, S.D., FOXFORD, K.A., WALSH, J.J., AND MARSHALL, J., 2001, An exhumed palaeo-hydrocarbon migration fairway in a faulted carrier system, Entrada Sandstone of SE Utah, USA: Geofluids, v. 1, p. 195–213.

GARRIDO, A.C. 2010, Estratigrafía del Grupo Neuquén, Cretácico Superior de la Cuenca Neuquina (Argentina): nueva propuesta de ordenamiento litoestratigráfico: Museo Argentino de Ciencias Naturales, Revista, v. 12, p. 121–177.

GIUSIANO, A., AND BOUHIER, E., 2009, Mineralización de Cu en el Grupo Neuquén vinculada a la migración de hidrocarburos. Dorso de los Chihuidos, Neuquén, Argentina: Boletín de Informaciones Petroleras, v. 11, p. 6–18.

GIUSIANO, A., FRANCHINI, M., IMPICCINI, A., AND O'LEARY, S., 2006, Mineralización de Cu asociada a bitumen en las areniscas cretácicas, prospecto Barda González, Neuquén, Argentina: XI Congreso Geológico Chileno, v. 2, p. 255–258.

GIUSIANO, A., FRANCHINI, M.B., IMPICCINI, A., AND PONS, M.J., 2008, Mineralización de Cu en sedimentitas Mesozoicas del Grupo Neuquén y hábitat de los hidrocarburos en la Dorsal de Huincul, Neuquén: XVII Congreso Geológico Argentino, v. 2, p. 769–770.

GIUSIANO, A., MENDIBERRI, H., AND CARBONE, O., 2011, Introducción a los Recursos Hidrocarburíferos, in Leanza, H.A., Arregui, C., Carbone, O., Danieli, J.C., and Vallés, J.M., eds., Geología y Recursos Naturales de la Provincia de Neuquén: XVIII Congreso Geológico Argentino, p. 639–644.

GIUSIANO, A., CEVALLOS, M., FRANCHINI, M., CARBONE, O., AND RAINOLDI, A., in press, Edivencias de la circulación de hidrocarburos a través del Grupo Neuquén (Cretácico Superior) en el Dorso de los Chihuidos, Cuenca Neuquina (abstract): XIX Congreso Geológico Argentino, 2 p.

GOLDHABER, M.B., REYNOLDS, R.L., CAMPBELL, J.A., WANTY, R.B., GRAUCH, R.I., AND NORTHROP, R., 1990, Part II. Mechanism of ore and gangue mineral formation at the interface between brine and meteoric water, in Northrop, H.R., and Goldhaber, M.B., eds., Genesis of the Tabular-Type Vanadium–Uranium Deposits of the Henry Basin, Utah: Economic Geology, v. 85, p. 236–250.

GONZÁLEZ-ACEBRÓN, L., ARRIBAS, J., AND MAS, R., 2010, Role of sandstone provenance in the diagenetic albitization of feldspars. A case study of the Jurassic Tera Group sandstones (Cameros Basin, NE Spain): Sedimentary Geology, v. 229. p. 53–63.

HERRERO DUCLOX, A., 1939, Estratigrafía y tectónica de los Estratos de Dinosaurios del Neuquén: Boletín Informativo Petrolero, v. 16, p. 16–17.

HERRERO DUCLOUX, A., 1946, Contribución al conocimiento geológico del Neuquén extrandino: Boletín Informativo Petrolero, v. 23, p. 1–39.

HIRT, W.G., WENK, H.R., AND BOLES, J.R., 1993, Albitization of plagioclase crystals in the Stevens sandstone (Miocene), San Joaquin Basin, California, and the Frio Formation (Oligocene), Gulf Coast, Texas: A TEM/AEM study: Geological Society of America, Bulletin, v. 105, p. 708–7014.

KAY, S.M., AND COPELAND, P., 2006, Early to Middle Miocene backarc magmas of the Neuquén Basin: geochemical consequences of slab shallowing and the westward drift of South America, in Kay, S.M., and Ramos, V.A., eds., Evolution of an Andean margin: A Tectonic and Magmatic View from the Andes to the Neuquén Basin (35°–39°S lat): Geological Society of America, Special Paper 407, p. 185–213.

KAY, S.M., GORRING, M., AND RAMOS, V.A., 2004, Magmatic sources, setting and causes of Eocene to Recent Patagonian plateau magmatism (36°S to 52°S latitude): Asociación Geológica Argentina, Revista, v. 59, p. 556–568.

LANGMUIR, D., 1997, Aqueous Environmental Geochemistry: New Jersey, Prentice-Hall, 600 p.

LANSON, B., BEAUFORT, D., BERGER, G., PETIT, S., AND LACHARPAGNE J.C., 1995, Evolution de la structure cristallographique des minéraux argileux en réponse aux conditions de température: exemple de l'illitisation des kaolins dans les réservoirs gréseux Rotliegend (Lower Slochteren–Permien inférieur), offshore des Pays Bas: Bulletin des Centres de Recherche Exploration-Production Elf Aquitaine, v. 19, p. 243–265.

LARTER, S., HUANG, H., ADAMS, J., BENNET, B., JOKANOLA, O., OLDENBURG, T., JONES, M., HEAD, I., RIEDIGER, C., AND FOWLER, M., 2006, The controls on the composition of biodegraded oils in the deep subsurface: Part II, Geological controls on subsurface biodegradation fluxes and constraints on reservoir-fluid property prediction: American Association of Petroleum Geologists, Bulletin, v. 90, p. 921–938.

LEANZA, H., AND HUGO, C., 2001, Cretaceous beds from southern Neuquén Basin (Argentina): age, distribution and stratigraphic discontinuities, in VII International Symposium on Mesozoic Terrestrial Ecosystems: Asociación Paleontológica Argentina, Special Publication 7, p. 117–122.

LEE, M.K., AND BETHKE, C., 1994, Groundwater flow, late cementation and petroleum accumulation in the Permian Lyons sandstones and its role in oil accumulation: American Association of Petroleum Geologists, Bulletin, v. 78, p. 217–237.

LEGARRETA, L., AND GULISANO, C.A., 1989, Análisis estratigráfico secuencial de la Cuenca Neuquina (Triásico Superior–Terciario Inferior, Argentina), in Chebli, G., and Spaletti, L., eds., Cuencas Sedimentarias Argentinas: Serie Correlación Geológica 6, p. 221–243.

LEGARRETA, L., LAFFITTE, G.A., AND MINNITI, S., 1999, Cuenca Neuquina: múltiples posibilidades en las series jurásico–cretácicas del depocentro periandino, in Chebli, G.A., ed., Actas: IV Congreso Exploración y Desarrollo de Hidrocarburos, v. 1, p. 145–175.

LEGARRETA, L., VILLAR, H.J., LAFFITE, G.A., CRUZ, C.E., LAFFITTE, G.A., AND VARADÉ, R., 2008, Revisión integrada de los sistemas generadores, estilos de migración-entrampamiento y volumetría de hidrocarburos en los distritos productivos de la Cuenca Neuquina, Argentina, in Cruz, C.E., Rodríguez, J.F., Hechem, J.J., and Villar, H., eds., Sistemas Petroleros de las Cuencas Andinas: VII Congreso de Exploración y Desarrollo de Hidrocarburos, p. 79–108.

LEVANDOWSKI, D.W., KALEY, M.E., SILVERMAN, S.R., AND SMALLEY, R.G., 1973, Cementation in Lyons sandstone and its role in oil accumulation, Denver Basin Colorado: American Association of Petroleum Geologists, Bulletin, v. 57, p. 2217–2244.

LITTKE, R., BRAUCKMANN F.J., RADKE, M., AND SCHAEFER, R.G., 1996, Solid bitumen in Rotliegend gas reservoirs in northern Germany: implications for their thermal and filling history: Zentralblatt für Geologie und Paläontologie, Teil 1, v. 11, p. 1275–1292.

MADEJOVÁ, J., BALAN, E., AND PETIT, S., 2011, Application of vibrational spectroscopy to the characterization of phyllosilicates and other industrial minerals, in Christidis, G.E., ed., Advances in the Characterization of Industrial Minerals: Notes in Mineralogy, v. 9, p. 171–226.

MAGOON, L.B., AND BEAUMONT, E.A., 1999, Petroleum system, in Beaumont, E.A., and Foster, N.H., eds., Exploring for Oil and Gas Traps: American Association of Petroleum Geologists, Treatise of Petroleum Geology, Chapter 3, p. 1–34.

MARETTO, H., AND PÁNGARO, F., 2005, Edad de formación de algunas de las grandes estructuras del engolfamiento de la Cuenca Neuquina: actividad tectónica durante la depositación de la Fm. Quintuco: VI Congreso de Exploración y Desarrollo de Hidrocarburos, CD-ROM, 11 p.

MCBRIDE, E.F., 1989, Quartz cement in sandstones: a review: Earth-Science Reviews, v. 26, p. 69–112.

MESSAGER, G., NIVIÉRE, B., MARTINOD, J., LACAN, P., AND XAVIER, J.P., 2010, Geomorphic evidence for Plio-Quaternary compression in the Andean foothills of the southern Neuquén Basin, Argentina: Tectonics, v. 29, p.TC4003.

MIALL, A., 1996, The Geology of Fluvial Deposits: New York, Springer, 582 p.

MOORE, D.M., AND REYNOLDS, R.J.R., 1997, X-Ray Diffraction and the Identification and Analysis of Clay Minerals: New York, Oxford University Press, 378 p.

MOSQUERA, A., AND RAMOS, V.A., 2006, Intraplate deformation in the Neuquén Embayment, in Kay, S.M., and Ramos, V.A., eds., Evolution of an Andean Margin: A tectonic and Magmatic View from the Andes to the Neuquén Basin (35°–39°S lat): Geological Society of America, Special Paper 407, p. 97–123.

NORTHROP, H.R., GOLDHABER, M.B., WHITNEY, G., LANDIS, G.P., AND RYE, R.O., 1990, Part III. Evidence from the mineralogy and geochemistry of clay minerals, in Northrop, H.R., and Goldhaber, M.B., eds., Genesis of the Tabular-Type Vanadium–Uranium Deposits of the Henry Basin, Utah: Economic Geology, v. 85, p. 250–269.

PARNELL, J., AND CAREY, P.F., 1995, Emplacement of bitumen (asphaltite) veins in the Neuquén Basin, Argentina: American Association of Petroleum Geologists, Bulletin, v. 79, p. 1798–1816.

PARRY, W.T., CHAN, M.A., AND NASH, B.P., 2009, Diagenetic characteristics of the Jurassic Navajo Sandstone in the Covenant oil field, central Utah thrust belt: American Association of Petroleum Geologists, Bulletin, v. 93, p. 1039–1061.

PITTMAN, E., 1979, Porosity, diagenesis and productive capability of sandstone reservoirs, in Scholle, P.A., and Schluger, P.R., eds., Aspects of Diagenesis: SEPM, Special Publication 26, p. 159–163.

PONS, M.J., FRANCHINI, M.B., GIUSIANO, A., IMPICCINI, A., AND GODEAS, M., 2009, Alteraciones, mineralización de Cu y Bitumen en areniscas Cretácicas del Prospecto Barda González, Neuquén, Argentina: Asociación Geológica Argentina, Revista, v. 64, p. 321–333.

PONS, M.J., FRANCHINI, M., CESARETTI, N., RAINOLDI, A., IMPICCINI, A., AND GIUSIANO, A., 2012, Relación entre los procesos diagenéticos y la migración de hidrocarburos en la Formación Portezuelo, Dorsal de Huincul, Neuquén (abstract): XIII Reunión Argentina de Sedimentología, p. 177–178.

RAINOLDI, A.L., FRANCHINI, M.B., CESARETTI, N.N., IMPICCINI, A., AND PONS, M.J., 2012a, Alteración y decoloración de areniscas rojas, Formación Huincul (Grupo Neuquén). Evidencias de la circulación de hidrocarburos en el Dorso de los Chihuidos (abstract): XIII Reunión Argentina de Sedimentología, p. 183–184.

RAINOLDI, A.L., LIMARINO, C.O., GIUSIANO, A., AND BOUHIER, E., 2012b, Análisis estratigráfico de la Formación Huincul (Grupo Neuquén) en el prospecto Sapo Sur (37°47′S–69°27′O), Dorso de los Chihuidos, Neuquén (abstract): XIII Reunión Argentina de Sedimentología, p. 185–186.

RAMOS, V.A., 1981, Descripción geológica de la hoja 33c Los Chihuidos Norte, Provincia de Neuquén: Servicio Geológico Nacional, Boletín, v. 182, p. 1–103.

RAMOS, V.A., AND BARBIERI, M., 1989, El volcanismo Cenozoico de Huantrairco: Edad y relaciones isotópicas iniciales, provincia del Neuquén: Asociación Geológica Argentina, Revista, v. 53, p. 210–223.

RAMOS, V.A., AND FOLGUERA, A., 2005, Tectonic evolution of the Andes of Neuquén: Constraints derived from the magmatic arc and foreland deformation, in Veiga, G.D., Spalletti, L.A., Howell, J.A., and Schwarz, E., eds., The Neuquén Basin: A Case Study in the Sequence Stratigraphy and Basin Dynamics: Geological Society of London, Special Publication 252, p. 15–35.

RAMOS, V.A., AND KAY, S.M., 2006, Overview of the tectonic evolution of the southern Central Andes of Mendoza and Neuquén (35°–39°S latitude), in Kay, S.M., and Ramos, V.A., eds., Evolution of an Andean Margin: A Tectonic and Magmatic View from the Andes to the Neuquén Basin (35°–39°S lat): Geological Society of America, Special Paper 407, p. 1–17.

RHEA, L., PERSON, M., DE MARSILY, G., LEDOUX, E., AND GALLI, A., 1994, Geostatistical models of secondary oil migration within heterogeneous carrier beds: a theoretical example: American Association of Petroleum Geologists, Bulletin, v. 78, p. 1679–1691.

RODUIT, N., 2008, JMicroVision: Image Analysis Toolbox for Measuring and Quantifying Components of High-definition Images. Version 1.2.7. Software available for free download at http://www.jmicrovision.com.

ROONEY, M., VALENTE, S., VULETICH, A., AND RENNISON, C., 1999, CO_2 origin and reservoir compartmentalization in the Sierra Chata Field, Neuquén Basin, Argentina, in Schoell, M., and Claypool, G.E., eds., Proceedings Hedberg Research Conference on "Natural Gas Formation and Occurrence," Durango, Colorado, 3 p.

ROWE, R.D., AND BURLEY, S.D., 1997, Faulting and porosity mofification in the Sherwood sandstone at Alderey Edge, north-eastern Chesire: an exhumed example of fault-related diagenesis, in Meadows, N.S., Trueblood, S.P., Hardman, M., and Cowen, G., eds., Petroleum Geology of the Irish Sea and Adjacent Areas: Geological Society of London, Special Publication 124, p. 325–352.

SALMINEN, R., BATISTA, M.J., BIDOVEC, M., DEMETRIADES, A., DE VIVO, B., DE VOS, W., DURIS, M., GILUCIS, A., GREGORAUSKIENE, V., HALAMIC, J., HEITZMANN, P., LIMA, A., JORDAN, G., KLAVER, G., KLEIN, P., LIS, J., LOCUTURA, J., MARSINA, K., MAZREKU, A., O'CONNOR, P.J., OLSSON, S.Å., OTTESEN, R.-T., PETERSELL, V., PLANT, J.A., REEDER, S., SALPETEUR, I., SANDSTRÖM, H., SIEWERS, U., STEENFELT, A., AND TARVAINEN, T., 2005, Geochemical Atlas of Europe, Part 1, Background Information, Methodology and Maps: Geological Survey of Finland, 526 p.

SÁNCHEZ, M., AND CARDOZO, J., 2002, Sedimentología y paleoambientes sedimentarios de la Formación Candeleros (Subgrupo Río Limay), Cretácico Tardío, sudeste del Neuquén: V Congreso de Exploración y Desarrollo de Hidrocarburos, CD-ROM, 8 p.

SÁNCHEZ M.L., ROSSI, J., MORRA, S., AND ARMAS, P., 2008, Análisis estratigráfico secuencial de las formaciones Huincul y Lisandro del Subgrupo Río Limay (Grupo Neuquén–Cretácico tardío) en el Departamento El Cuy, Rio Negro, Argentina: Latin American Journal of Sedimentology and Basin Analysis, v. 15, p. 1–26.

SCASSO, R.A., AND LIMARINO, C.O., 1997, Petrología y Diagénesis de Rocas Clásticas, Second Edition: Asociación Argentina de Sedimentología, Special Publication 1, 257 p.

SCHÖNER, R., AND GAUPP, R., 2005, Contrasting red bed diagenesis: the southern and northern margin of the Central European Basin: International Journal of Earth Sciences, v. 94, p. 897–916.

SCHUMACHER, D., 1996, Hydrocarbon-induced alteration of soils and sediments, in Schumacher, D., and Abrams, M.A., eds., Hydrocarbon Migration and its Near-Surface Expression: American Association of Petroleum Geologists, Memoir 66, p. 71–89.

SHEBL, M.A., AND SURDAM, R.C., 1996, Redox reactions in hydrocarbon clastic reservoirs: experimental validation of this mechanism for porosity enhancement: Chemical Geology, v. 132, p. 103–117.

SURDAM, R.C., BOESE, S.W., AND CROSSEY, L.J., 1984, The chemistry of secondary porosity, in McDonald, O., and Surdam, R., eds., Clastic Diagenesis: American Association of Petroleum Geologists, Memoir 37, p. 127–149.

SURDAM, R.C., CROSSEY, L.J., HAGEN, E.S., AND HEASLER, H.P., 1989, Organic–inorganic interactions and sandstone diagenesis: American Association of Petroleum Geologists, Bulletin, v. 73, p. 1–32.

SURDAM, R.C., JIAO, Z.S., AND MACGOWAN, D.B., 1993, Redox reactions involving hydrocarbons and mineral oxidants: a mechanism for significant porosity enhancement in sandstones: American Association of Petroleum Geologists, Bulletin, v. 77, p. 1509–1518.

TUNIK, M., PONS, J., PIMENTEL, M., AND RAMOS, V.A., 2008, Procedencia de los depósitos sinorogénicos del Grupo Neuquén (cuenca neuquina del sur de Mendoza y Neuquén) (abstract): XVII Congreso Geológico Argentino, v. 3, p. 1310–1311.

UGARTE, F.R.E., 1976, Teoría de la fracturación de un yacimiento fisurado de hidrocarburos (Aguada San Roque), Provincia del Neuquén: VI Congreso Geológico Argentino, no. 6, p. 307–317.

VELDE, B., 1985, Clay Minerals: A Physico-Chemical Explanation of Their Occurrence: Amsterdam, Elsevier, Developments in Sedimentology, no. 40, 427 p.

VERGANI, G.D., TANKARD, A.J., BELOTTI, H.J., AND WELSINK, H.J., 1995, Tectonic evolution and paleogeography of the Neuquén Basin, Argentina, *in* Tankard, A.J., Suárez, S.R., and Welsink, H.J., eds., Petroleum Basins of South America: American Association of Petroleum Geologists, Memoir 62, p. 383–402.

VERGANI, G., ARREGUI, C., AND CARBONE, O., 2011, Sistemas petroleros y tipos de entrampamientos en la Cuenca Neuquina, *in* Leanza, H.A., Arregui, C., Carbone, O., Danieli, J.C., and Vallés, J.M., eds., Geología y Recursos Naturales de la Provincia de Neuquén: XVIII Congreso Geológico Argentino, p. 645–656.

WALKER, T.R., 1989, Application of diagenetic alterations in red beds to the origin of copper in stratiform copper deposits, *in* Boyle, R.W., Brown, A.C., Jefferson, C.W., Jowett, E.C., and Kirkham, R.V., eds., Sediment-Hosted Stratiform Copper Deposits: Geological Association of Canada, Special Paper 36, p. 85–96.

WORDEN, R.H., AND BURLEY, S.D., 2003, Sandstone diagenesis: the evolution from sand to stone, *in* Burley, S.D., and Worden, R.H., eds., Clastic Diagenesis: Recent and Ancient: International Association of Sedimentologists, v. 4, p. 3–44.

WORDEN, R.H., AND MORAD, S., 2000, Quartz cementation in oil field sandstones: a review of the key controversies, *in* Worden, R.H., and Morad, S., eds., Quartz Cementation in Sandstones: International Association of Sedimentologists, Special Publication 29, p. 1–20.

YU, K.M., BOGGS, S., SEYEDILALI, A., AND KO, J., 1997, Albitization of feldspars in sandstones from the Gohan (Permian) and Donggo (Permo-Triassic) Formations, Gohan area, Kangwondo, Korea: Geosciences Journal, v. 1, p. 26–31.

ZAMORA VALCARCE, G., ZAPATA, T., RAMOS, V.A., RODRÍGUEZ, F., AND BERNARDO, L.M., 2009, Evolución tectónica del frente Andino en Neuquén: Asociación Geológica Argentina, Revista, v. 65, p. 192–203.